CHARGE SEPARATION ASSOCIATED WITH FROST GROWTH

by

JAMES PETER RYDOCK

S. B., Physics
Massachusetts Institute of Technology
(1985)

SUBMITTED TO THE DEPARTMENT OF
EARTH, ATMOSPHERIC, AND PLANETARY SCIENCES
IN PARTIAL FULFILLMENT OF THE REQUIREMENTS FOR
THE DEGREE OF

MASTER OF SCIENCE IN METEOROLOGY

at the

MASSACHUSETTS INSTITUTE OF TECHNOLOGY

February 1989

Signature of Author_____
Department of Earth, Atmospheric, and Planetary Sciences
November 3, 1988

Certified by_____
Earle R. Williams
Thesis supervisor

Accepted by_____
Thomas H. Jordan
Department Chairman

CHARGE SEPARATION ASSOCIATED WITH FROST GROWTH

by

JAMES PETER RYDOCK

Submitted to the Department of Earth, Atmospheric,
and Planetary Sciences on November 3, 1988
in partial fulfillment of the requirements for the Degree of
Master of Science in Meteorology

ABSTRACT

Measurements are made of the electrical charge transfer from cold objects immersed in warm and humid environments. In three sets of experimental runs with a cold (<0°C) 6" diameter stainless steel sphere (STS), one each at chamber temperatures (T_C) = 28°C, 41°C, and 52°C in high humidity, it is found that the electrical current associated with frost growth increases to a well defined maximum value (I_{max}) in a finite time (t_{imax}), followed by an exponential decay of the current to zero. A second current signature associated with the melting of the accumulated frost is observed as the sphere warms through 0°C. Maximum currents range from .5 to 10 pA, with systematic transfer of negative charge from the sphere. I_{max} and t_{imax}^{-1} are a strong function of the initial temperature (T_S) of STS, both quantities increasing with decreasing T_S above -50°C to a maximum near -15°C followed by a decrease up to T_S=0°C. This temperature (T_S) dependance for I_{max} is largely independent of chamber condition, but all I_{max} values increase markedly with T_C and the absolute humidity. This general behavior is also exhibited by copper and aluminum specimens used as the substrate for frost growth.

It is found that the charge carriers are miniscule ice particles ejected primarily from a limited area on the bottom-facing region of a specimen during frost growth. Supplemental experiments with prefrosted metal substrates, which yield currents an order of magnitude smaller than with clean metal substrates, suggest that surface effects are involved, but probably not a thermoelectric effect. It is hypothesized that the separation current is proportional to the rate of fragment ejection, and that the ejection is a function of the growth rate of ice on the 'active' areas, but with limited microphysical information firm conclusions are not possible.

The estimated temperature and vapor gradients at the surface in these experiments are 2-3 orders of magnitude larger than those experienced by graupel particles falling in a thundercloud, and the stainless steel sphere is two orders of magnitude larger than a realistic atmospheric hydrometeor. Thus, in light of the magnitude of the currents measured, we are skeptical about the direct role for this phenomena in atmospheric charge separation. However, an understanding of the importance of this charge separation phenomenon at the molecular scale warrants further study.

Thesis supervisor: Earle R. Williams

Title: Assistant Professor of Meteorology

Table of Contents

Acknowledgements

The primary acknowledgement for this work is to Earle Williams, for providing many thoughts and ideas (the biggest of which was the study of the phenomena in the first place), and also for continually pointing me in the right direction, however much I fight it. I would also like to acknowledge Speed Geotis and Oliver Newell for help with work in the laboratory, and Curtis Tsai for electrical suggestions.

Biographical Note

The author, Jim Rydock, was born in Milwaukee, WI, and was raised there and in Elizabethtown, PA. He received an S.B. Degree in Physics from MIT in 1985, and temporarily resides in Somerville, MA.

Introduction

It has become increasingly clear that an understanding of the microphysical properties of ice is essential in unraveling the mystery of large scale charge separation and lightning in thunderclouds. Experiments to simulate processes involving the ice phase in the atmosphere are difficult to devise and interpret because of the physical constraints of the laboratory, and thus have received only intermittent attention through the years. Because of this, very much remains unknown about the specific roles of ice in atmospheric charge separation. In this paper, we study the charge transfer associated with frost growth to a simulated hydrometeor in the laboratory in an attempt to contribute to the solution of this problem.

Recent experimental work in this field has focused on charge transfer during interactions between a simulated graupel particle and vapor-grown ice crystals. Jayaratne, et al (1983), whirled a rimed stainless steel rod through an environment of supercooled water and ice crystals. They found that no measurable charge was transferred in an environment of supercooled water only, and that the rod charged slightly negatively at high rotation speeds when ice crystals alone were present, but slightly positively if frost was growing on the rod. Much larger signals were observed when both crystals and supercooled water were present, and it was found that the sign and magnitude of the charge separation was strongly dependent on temperature and liquid water content in the experiment chamber. Generally, the rod charged positively at higher

temperatures and higher liquid water contents and negatively at lower temperatures and lower liquid water contents. The charge reversal temperature was found to be between -10 and -20 degrees Celsius, depending on LWC.

Baker, et al., (1987) repeated and extended the above measurements to a wider range of temperature values (-1.5 °C to -35 °C) and obtained results consistent with Jayaratne, et al., (1983). These workers suggested that the important microphysical property for significant charge separation is that the ice crystals and simulated soft hailstone be growing by the diffusion of vapor supplied by evaporation of the supercooled water droplets present. Also, it was hypothesized that it is the relative growth rates, by diffusion, of the crystals and the target which determine the sign of the transfer. Calculations of growth rates yielded results which are not inconsistent with the idea that the simulated hydrometeor charges positively when it is growing faster than the ice crystals in the cloud and negatively when the crystals are growing faster. However, no specific microphysical explanation was given to account for these observations.

Caranti, Illingworth, & Marsh (1985) impacted 100 micron ice spheres on various metal targets and found that the sign and magnitude of the charge transferred in such interactions were dependent on the work function of the metal and also on the growth state of the target, i.e. whether or not frost was growing or evaporating from the metal surface. Generally, when the target was growing by vapor deposition, collisions left it with a positive charge. Conversely, when evaporating, impacting ice spheres deposited a negative charge. They attributed these effects to

differences in contact potentials between the surfaces, leading to charge transfer when in contact during the collisions.

The researchers in the above experiments were interested principally in the ice-particle collisions and not the electrical characteristics of frost growth and evaporation alone. Latham (1963) exposed a frost specimen, grown by deposition from the vapor, to airstreams of different temperatures and noted that, generally, the ice whiskers blown off were charged positively when the airstream was colder than the frost and negatively when the airstream was warmer. He attributed this charge separation to a thermoelectric effect in ice, first proposed by Latham and Mason (1961), driven by the temperature gradient between the frost and the airstream. It is well known that the mobile charge carriers in ice are H^+ and OH^- ions and that H^+ ions have a much higher mobility. Also, the number of mobile charge carriers is a function of temperature. Hence, positive ions should diffuse down the temperature gradient faster than OH^- ions, leading to an excess positive charge in the colder section and an excess negative charge in the warmer area. Thus, whiskers blown off the surface will have a charge determined by the imposed temperature gradient.

In later work, Latham and Stow (1965), suggested that evaporation of ice should, because of latent heat considerations, result in a cooling at the surface and a subsequent interior temperature gradient yielding a thermoelectric charge separation in the manner above. Hence, evaporation should carry away positive charge, leaving a specimen with a net negative charge. Experiments to confirm this were done with a smooth ice surface

subjected to a dry nitrogen stream at various temperatures. Though the results yielded charge transfers of a sign consistent with the above ideas, further work by Latham and Stow (1966) showed that it is energetically impossible for molecules to be carrying the observed amount of charge away during evaporation, even if all of the charge thermoelectrically separated did indeed reside on the ice surface.

By qualitative reasoning similar to that above, a thermoelectric effect should produce a net positive charge on a specimen growing by vapor deposition. We suspect Latham and Stow did not consider this because they were not aware of any removal of particles from a growing ice specimen. However, Schaefer and Cheng (1971) observed that dendritic frost growth from deposition and riming to a simulated graupel particle placed in a warm, moist environment was accompanied by ejection and fragmentation of ice crystals from the frosty surface. Microscopic observations suggested that strong electrical effects were involved, with the dendrites twisting and turning and occassionally shooting off, and also that the crystal splintering occurred only during positive growth cycles. In these experiments, however, there was no attempt to quantify any charge separation or electric field variations.

To the best of our knowledge, there has been no research directed specifically at quantifying charge separation associated with frost growth from pure water vapor and cloud droplets, with no chemical contaminants involved and no particle collisions. It would seem that experiments to do so are a necessary step and perhaps more fundamental to the understanding of the microphysics of ice than collision experiments, which incorporate

several poorly understood effects simultaneously.

In this research, we attempt to make some progress in understanding the electrification associated with frost growth by extending Schaefer and Cheng's earlier work. Our goal is to measure the charge separation, as an electric current, from a cold simulated hydrometeor placed in warm and humid air. Then, to determine if and how the charge separation depends on the initial temperature, composition, and geometry of the simulated graupel particle, and on the temperature of the moist environment. And further, to gain insight into the nature of the processes responsible for the phenomenon.

Experiment

The principal experiments are conducted in a standard 55 gallon (.208 m^3) stainless steel drum used as a miniature cloud chamber, shown in Figure 1. The drum is covered on the outside with 1 inch fiberglass insulation secured with duct tape, and three Thermolyne heating tapes powered by variacs are used to achieve quasi-steady state temperatures in the chamber. Environments warmer than room temperature can be maintained and adjusted by varying the voltages to the tapes. A pan at the

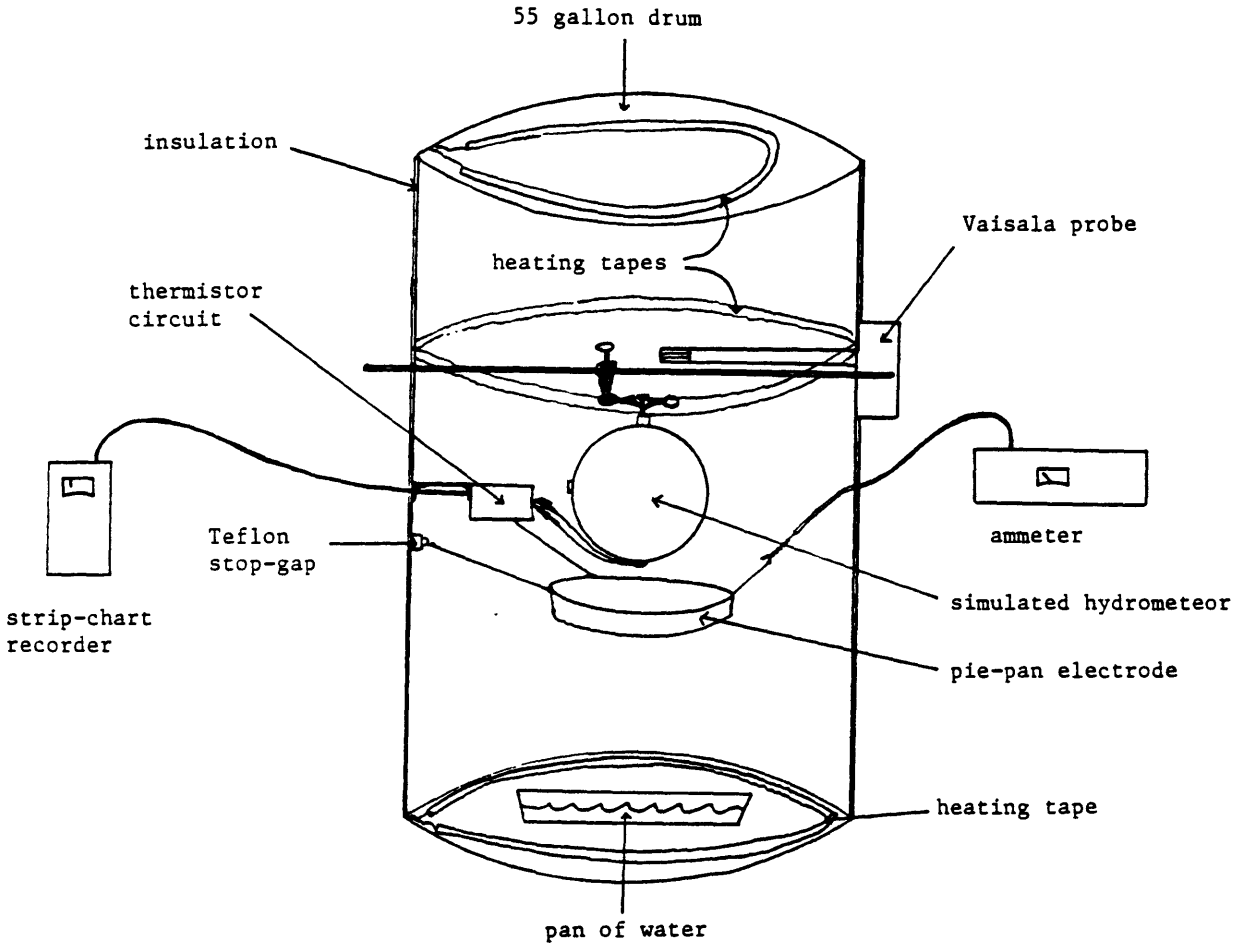

Figure 1 - Experiment chamber

bottom of the chamber is filled with water pre-heated to the environmental temperature to provide vapor for the frost growth. The temperature and relative humidity of the air in the can are continuously monitored with a Vaisala Series HMP 110A humidity probe mounted approximately 12 inches below the top of the drum.

Approximately level with the probe, a .375 inch diameter stainless steel rod is mounted through the drum and serves as the support for the cold simulated hydrometeor. A 9" diameter aluminum pie pan is centered several inches beneath the simulated hydrometeor to catch the splintering ice particles ejected and carried downward by gravity during frost growth. The pan is electrically connected to a Keithley Model 410 picoammeter and thus is an electrode for the measurement of charge separation. Runs with an ungrounded simulated hydrometeor connected directly to the ammeter yield numbers which are equal in magnitude but opposite in sign to the current measurements from the pie pan using a grounded specimen (An example of this is shown in Figure 21 in the Interpretation section). Thus, we are confident that the plate indeed collects all of the charge carriers separated during a trial. The pie pan method of measurement is preferred because of the ease and quickness it affords in placing the simulated hydrometeor into the chamber and beginning a run. The pan-electrode is mechanically supported by strands of waxed dental floss tied to two .5" Teflon insulators glued to the drum wall. The Teflon is sufficient to prevent leakage currents because there is no liquid water near the chamber wall at any time during an experimental run. Occassionally, the Teflon must be washed with acetone to remove hygroscopic dirt particles which

accumulate on the insulator surface.

The ammeter is located outside the chamber and its input BNC is grounded to the metal drum, providing good shielding for the pan-electrode The Keithley instrument has twenty settings between $10X10^{-4}$ Amps and $3X10^{-13}$ Amps with an output of 0 to 5 volts full scale at each setting. A millivolt electrometer measures the voltage drop across input resistors to determine the current. High input impedance and shunt capacitors limit the e-folding response to about 1 second at the settings of interest (10^{-12} to 10^{-11} Amperes) for these experiments. The output of the ammeter is connected to a Rustrak strip chart recorder.

The principal simulated hydrometeor used is a welded 6" diameter hollow stainless steel sphere (STS), manufactured by Weil Pump Co., Chicago, IL, filled with water to approximately 91% of its capacity (about 1800 ml) and then frozen. The sphere is supported by a .25" diameter screw and thread assembly welded to the top. Other objects are used to explore the possible contaminating effect of metal type on the observed charge transfer. These include two six inch diameter hemispheric aluminum cups (made from type O 3003 Al by Carlstrom Pressed Metals, Inc., Worcester, MA, and subsequently referred to as AL1 and AL2) filled with 700 ml water and then frozen. Each is supported by three wires soldered through holes 120 degrees apart in the cup lip and centered and soldered together above to an alligator clip. 6" diameter hemispheres of ice, formed by freezing distilled water to plastic supports within the 6" aluminum cups, give a true ice surface to test for charge separation. And last, a 6" diameter aluminum sphere made from two welded aluminum cups

of the above type is used for comparison with the 6" stainless steel sphere. It is held up by a stainless steel hook attached to the top. Hence, during the experiments the metal simulated hydrometeors are grounded and so no charge can accumulate on their surfaces. The distilled water ice hemispheres, on the other hand, are floating electrically.

In the earliest experiments, a small (approximately 1.5" radius) copper planting cup supported by an alligator clip in the manner of the aluminum hemispheres was also used in a room temperature environment at high humidity and yielded results with the same general trends as the other metal simulated hydrometeors. Work with this specimen suggested that to get current values significantly above the noise of the ammeter for all test conditions, larger specimens and warmer chamber temperatures are desirable. This motivated the use of the larger 6" diameter stainless steel and aluminum simulated hydrometeors and the heating tapes for the main body of trials.

The simulated hydrometeors are frozen in a thermostat controlled So-Low brand chest freezer capable of -50 degrees Celsius. They are generally frozen overnight to ensure that equilibrium with the freezer has been reached. Metal hydrometeor temperatures in the freezer are monitored with Omega 44033 precision bead thermistors interchangeable to ±0.1 degrees C. The stainless steel sphere has two small hollowed stainless steel knobs welded to the outside, one at the equator and one on the bottom pole, where thermistors can be inserted and are removable. Similarly, the aluminum sphere has one hollowed aluminum knob welded to the equator. Thermistors sheathed and sealed in .875" sections of .125"

diameter copper piping, flattened and drilled at one end, can be screwed into holes at the lips of the aluminum cups for temperature determination. Unfortunately, a drawback of the distilled water ice hemispheres is the absence of a convenient means of accurately monitoring the surface temperature. In these experiments, we assumed that the ice temperature could be reasonably represented by the value of a thermistored, ice filled aluminum cup at the same height in the freezer.

A simple amplifier circuit (see Appendix A for diagram) in an aluminum shielding box is mounted to the inside wall of the drum and connected to a strip chart recorder. Alligator clips serve as the connector between the circuit and the leads of a thermistor attached to the metal simulated hydrometeor used during an experimental run. The time constant for the Omega 44033 is about 10 seconds in still air and the dissipation constant, defined as the power in milliwatts to raise a thermistor 1 °C above the surrounding temperature, is on the order of 1 mw/°C. Hence, the most important design consideration for the circuit is that it supply a minimal current to the thermistor. In this case it acts as a constant current source of approximately 15 microamps. The maximum resistance encountered in the experiments is 150 K, corresponding to about -50 °C. For this worst case, we have a power dissipation in the thermistor of .03 mW<< 1 mW, and therefore it can be neglected. Thus, a measure of the surface temperature during frost growth can be accurately and continuously recorded.

Finally, a small (.375" diameter) hole drilled in the side of the drum can be used, with the aid of a 40 Watt lamp set inside the chamber, to view the process of crystal splintering and ejection.

The typical procedure in an experimental run consists of first warming the drum to the desired temperature and then adding the heated water to build up the vapor supply to the desired level, which generally takes 30-45 minutes. It is important to allow the can to heat up for several hours before a run so that the drum walls and Teflon supports can come to equilibrium with the air temperature in the can. This prevents water from condensing on the insulators and causing leakage currents. When the appropriate relative humidity and temperature have been reached, a trace of the background current to the pie pan-electode is taken for several minutes to check for leakage currents and to determine the zero level on the Rustrak recorder. With this step successfully completed, the simulated hydrometeor, which has been cooled to the desired temperature, is quickly removed from the freezer and placed into the chamber. Generally, 15-20 seconds are consumed between opening the freezer door and getting a meaningful reading on the ammeter. Data is then taken until the frost grown on the simulated hydrometeor has melted.

There are obvious problems with the initial boundary conditions in this experiment. The procedure does not allow for rigorous reproducibility. In placing the cold object in the drum, the cover must be partially removed, allowing drier room temperature air to mix with the chamber environment. The degree of mixing is dependent on the temperature difference between the can and the outside and the length of time the lid is ajar. Also, the twenty odd seconds required for the transfer between the freezer and the chamber are lost data and represent an unknown variable which is not easily eliminated.

Probably more important than the variable initial condition, though, is the fact that the temperature of the cold object cannot be fixed during frost growth. In an experiment which is attempting to measure charge transfer vs. temperature at which ice is splintering, this is of crucial importance. However, the temperature difference between the simulated hydrometeor and the warm moist environment of the chamber is so great (30°C - 100°C) that, with this arrangement, it is impossible to maintain a constant ice temperature. The only temperature value that we are confident is a valid representation is the temperature of the surface of the object when it is in the freezer. Once in the drum, it becomes a complicated heat transfer problem. The warmup behavior of a simulated hydrometeor is geometry dependent, and is also a function of position on the surface, and the temperature and humidity of the growth environment. Temperature can be monitored at several points on the metal surfaces during ice growth, as has been described previously, but at best it is an approximation of the value at other points on the metal and at the tips of the growing dendrites.

This leads to an obvious question as to why the experiment is set up in this manner. Clearly, such large temperature gradients are never experienced by real graupel particles growing in a thunderstorm. We estimate that a graupel particle in a dry growth regime is probably never greater than 0.5°C warmer than its environment while falling through a thundercloud (For details see Appendix E). The exaggerated growth conditions also make analyses and conclusions very difficult. However, the most important consideration here is to be able to measure the

phenomenon with the instrumentation and equipment available, and it is within these constraints that the experiment evolved.

The main body of experiments is done with the chamber temperature (T_C) at 41 °C and the starting relative humidity (RH_S), before the cover is opened to place the cold object inside, at 88% (vapor content ≈ 50 gm/m^3). This combination is chosen because it is a relatively easy-to-achieve moist environment with a strong signal to noise ratio in the measured current. Runs are completed with the starting temperature of the cold object (T_S) ranging from -50°C all the way up to 0°C, in increments of 3 - 6°C, to test the dependence of the current measured on ice growth temperature. To establish repeatability and reliability, 3 or more trials at each starting temperature (T_S) are run for each of the simulated hydrometeors.

To test for the dependence of electrical current on different vapor concentrations, a less extensive set of experiments with the aluminum cups and the stainless steel sphere is conducted at Tc =28°C, RHs=93% (vapor content ≈ 26 gm/m^3), or about one half of the above value. Also, a set of current measurements is run a Tc =52°C, RHs =85%, vapor content ≈ 79 gm/m^3, or about 1.5 times the vapor content of the Tc=41°C runs, with the stainless steel sphere only. These additonal runs focus on the stainless steel simulated hydrometeor because, in the initial experiments, it was found that the current magnitudes from runs with this specimen appear more repeatable and consistent than for the other cold objects.

Data

In the course of the experiments it was found that certain systematic features of the current vs. time plots are common to all runs with the metal simulated hydrometeors at all temperatures where a signal is detected (ie. where the signal to noise ratio is greater than 1 at a particular ammeter setting). An example of a typical Rustrak trace is shown in Figure 2. This particular run was done at T_C =41°C, RH_S =88%, T_S=-20°C, with the 6" stainless steel sphere (STS). Four divisions horizontally is equal to fifteen minutes, and one large division in the vertical is .6 X 10^{-12} amps (In all of the Rustrak traces shown in this paper, five large divisions vertically are equal to the full scale of the instrument, and this number is always listed in the lower lefthand side of the trace). Negative charge from the sphere (and to the pie pan) is represented by a downward deflection and the background zero line is at the left. The run begins at the abrupt drop of the recorder needle. Discrete 'samples' on the Rustrak are separated by 2 seconds. The maximum current value of -1.7 pA to the pan-electrode is reached approximately 30 seconds into the experiment, as the simulated hydrometeor is charging positively. The current then tails off exponentially to zero at about 8 minutes and remains there until the 'spike' at the end of the run which is associated with the melting of the frost growth.

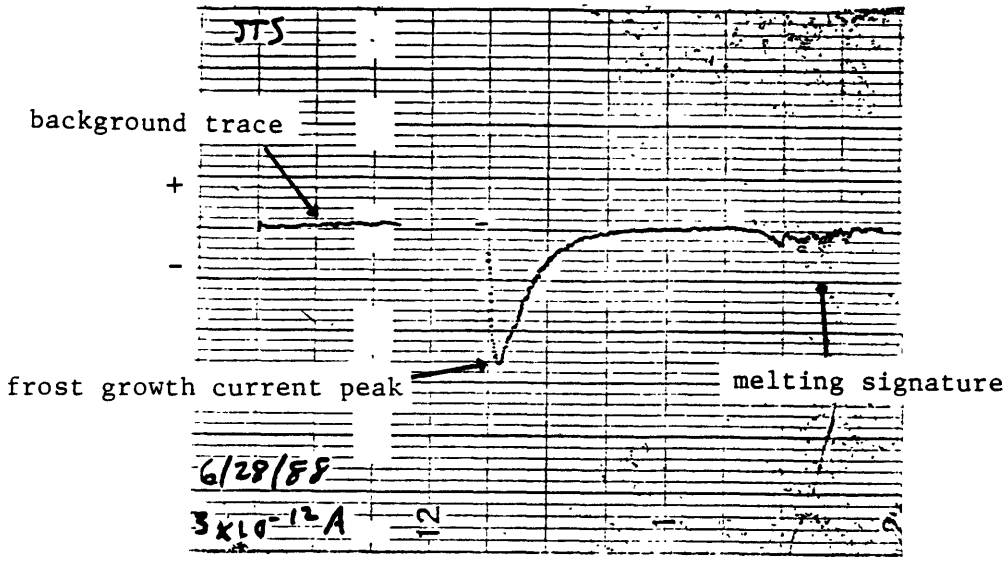

Figure 2 - Typical current trace for an experiment run, showing background current, peak associated with frost growth, and melting signature.

In all of the runs in which there is a measurable current (S/N >1), as in the example above, there is always a quick rise to the peak current at the start followed by an exponential decline to zero and then a second current maximum associated with melting that signifies the end of the experiment. The two peaks are mutually inclusive, i.e. both are seen or there is no charge transfer detected at all (S/N ≅1).

There are also systematic features to all sets of runs with a particular simulated hydrometeor at one chamber temperature. Generally, the maximum current increases with increasing temperature to some maximum value (T_{smax}) and then decreases above this temperature. The time to maximum current, on the other hand, tends to decrease with increasing temperature up to T_{smax} and then increases above this temperature. In other words, the highest peak currents are achieved in the shortest times.

Total run times increase with decreasing T_S at a given T_C and generally also increase with decreasing chamber temperature. These features are illustrated in Figure 3, which shows a partial set of runs done at T_C=28°C, RH_S=93%. Again, in all of the traces, negative charge to the pan is downward, five large divisions is equal to $10X10^3$ amps (1pA), and four divisions horizontally is 15 minutes. The runs start with a background trace at the left followed by the current profile. Note that the trial at T_S=-2°C is a straight line (S/N ≤1).

The finite time to maximum current does not seem to be a relic of the response time of the ammeter, but a real, systematic effect in the frost growth/charge separation process. The smoothness of the frost growth

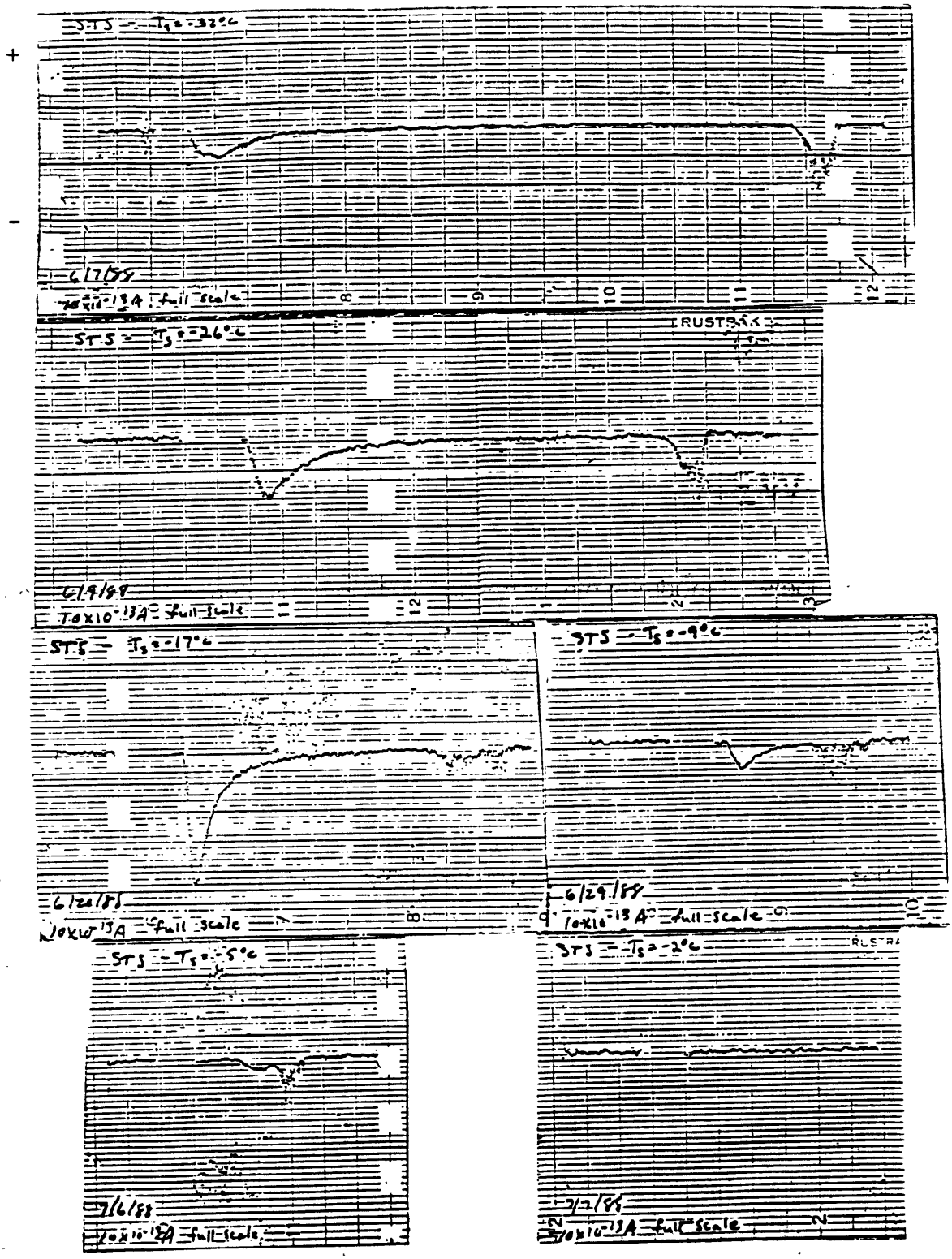

Figure 3 - Set of runs with STS at Tc=28°C, full scale = 1 pA.

peak suggests that the charge carriers from the simulated hydrometeor in this regime represent a near continuum of particles, whereas the melting signature appears to be a series of discrete events, recognizable within the response speed of the instrument. Also, in all of the runs using cold metal objects, the current to the pie pan is always negative (i.e. there is no temperature regime or time period during the growth and melting process in which there is a net transfer of positive charge from the simulated hydrometeors to the pie pan).

In the following we focus principally on the data from the stainless steel sphere, as it appears to be the most repeatable and consistent and thus amenable to analysis. Within the STS data we concentrate on the set of numbers from T_C=41°C, RH_S=88%, because this is where the greatest percentage of the trials are conducted.

A plot of the maximum pie pan current (I_{max}) in the frost growth peak vs. starting temperature (T_S) of the cold object for T_C =41°C, RH_S=88% is shown in Figure 4. Clearly, there is a strong and consistent dependence of I_{max} on T_S, with a pronounced peak around -17°C. I_{max} appears to decrease monotonically for temperatures on the cold side of -18°C down to the freezer limit of -50°C, where the values are about 20% of the maximum of -2.8 pA. I_{max} drops sharply for temperatures warmer than -17°C but there is evidence for a distinct 'shoulder' in the temperature dependence between -10°C and -5°C. There is also an abrupt cut-off regime between -5°C and -4°C, where the charge transfer drops to zero. At -5°C the frost

Figure 4 - Data from STS, Tc=41 C, RHs=88%

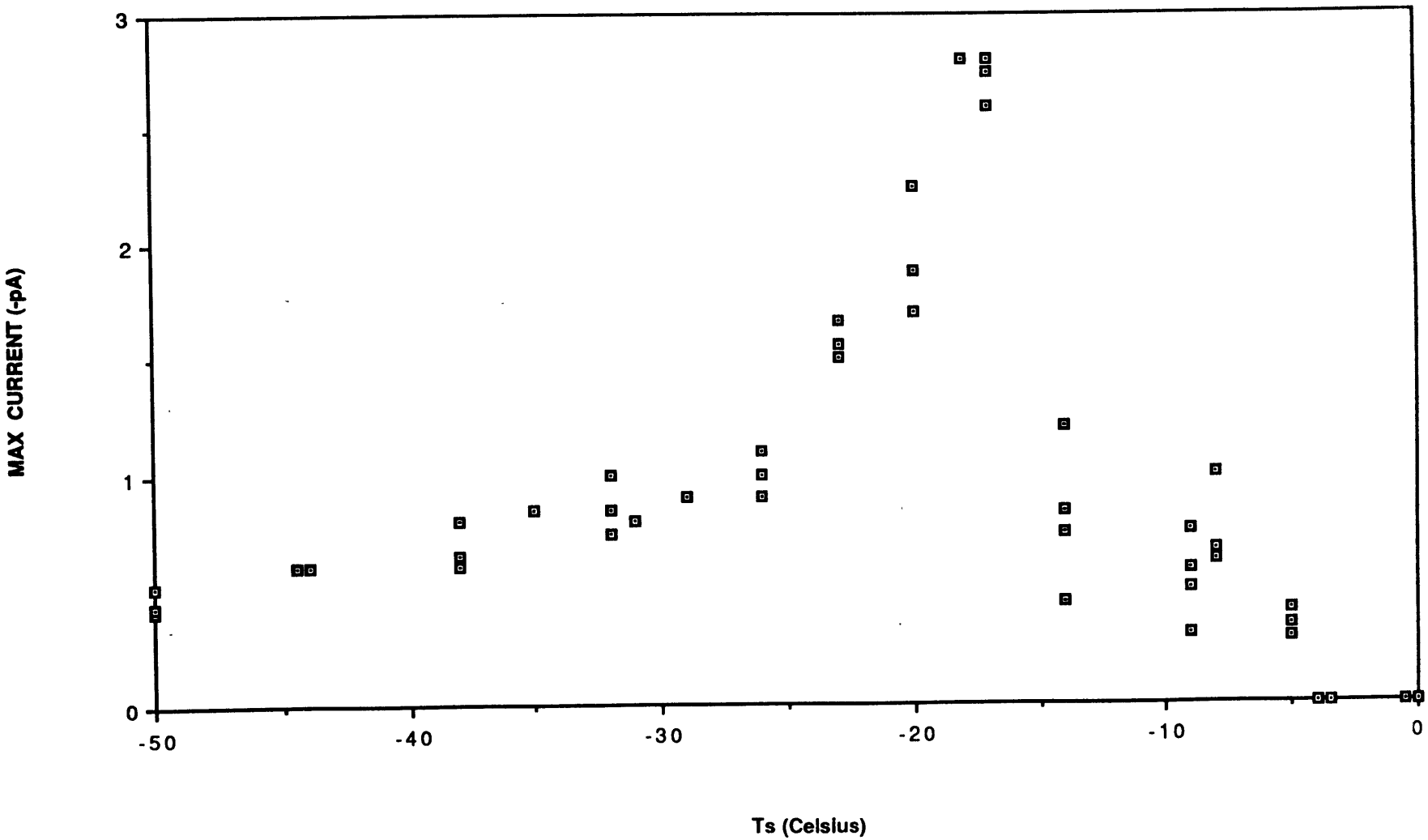

growth peak and the melting signature are distinguishable, while at -4°C the Rustrak trace is a straight line (S/N ≤1, similar to Fig. 3). Visual observations of these 'warm' T runs suggest that above -4°C no real frost growth and ejection of ice splinters occurs, just condensation on the metal surface.

Total run times between start and frost melt at 41°C for STS range from 60-70 minutes at T_S=-50°C down to about 7 minutes at T_S=-5 °C, where the growth peak and melting signature overlap.

For each of eleven T_S values,listed in Table 1, the times from the start of a run to I_{max} of that run (t_{imax}) from the current traces at that T_S are averaged to yield $\bar{t}_{imax}$, also listed in Table 1. $\bar{t}_{imax}$ is greatest (140 sec.) at T_S = -50°C and gradually shortens to a minimum value of about 35 seconds at -17°C. For T_S > -17°C, the average time to I_{max} then increases. These averages are also plotted in Figure 4A. Note, again, that the peak I_{max} value and the fastest $\bar{t}_{imax}$ occur at the same temperature.

For the experimental results plotted in Figure 4 there was no monitoring of the surface temperature of the stainless steel sphere, as the connection of the thermistor amplifier circuit to the simulated hydrometeor occassionally causes spurious current signals. Runs to determine temperature-time profiles of the warming stainless steel sphere were conducted in addition to the above, and the current measurements from these trials were discarded. The temperature history of the bottom of the sphere was taken for the eleven T_S values between

Table 1 - Time ($\bar{t}_{imax}$) and temperature ($\bar{T}_{bimax}$) at the bottom of STS at I_{max}, T_c=41°C, RH_s=88%

T_s (°C)	$\bar{t}_{imax}$ (sec)	$\bar{T}_{bimax}$ (°C)	$\bar{I}_{max}$ (pA)
-50	140	-44	.45
-44	98	-39	.60
-38	66	-34	.68
-32	58	-28	.86
-26	57	-22	1.00
-23	49	-19	1.57
-20	53	-16	1.94
-17	34	-13	2.72 *
-14	74	-10	.88
-9	113	-3	.56
-5	180	0	.34

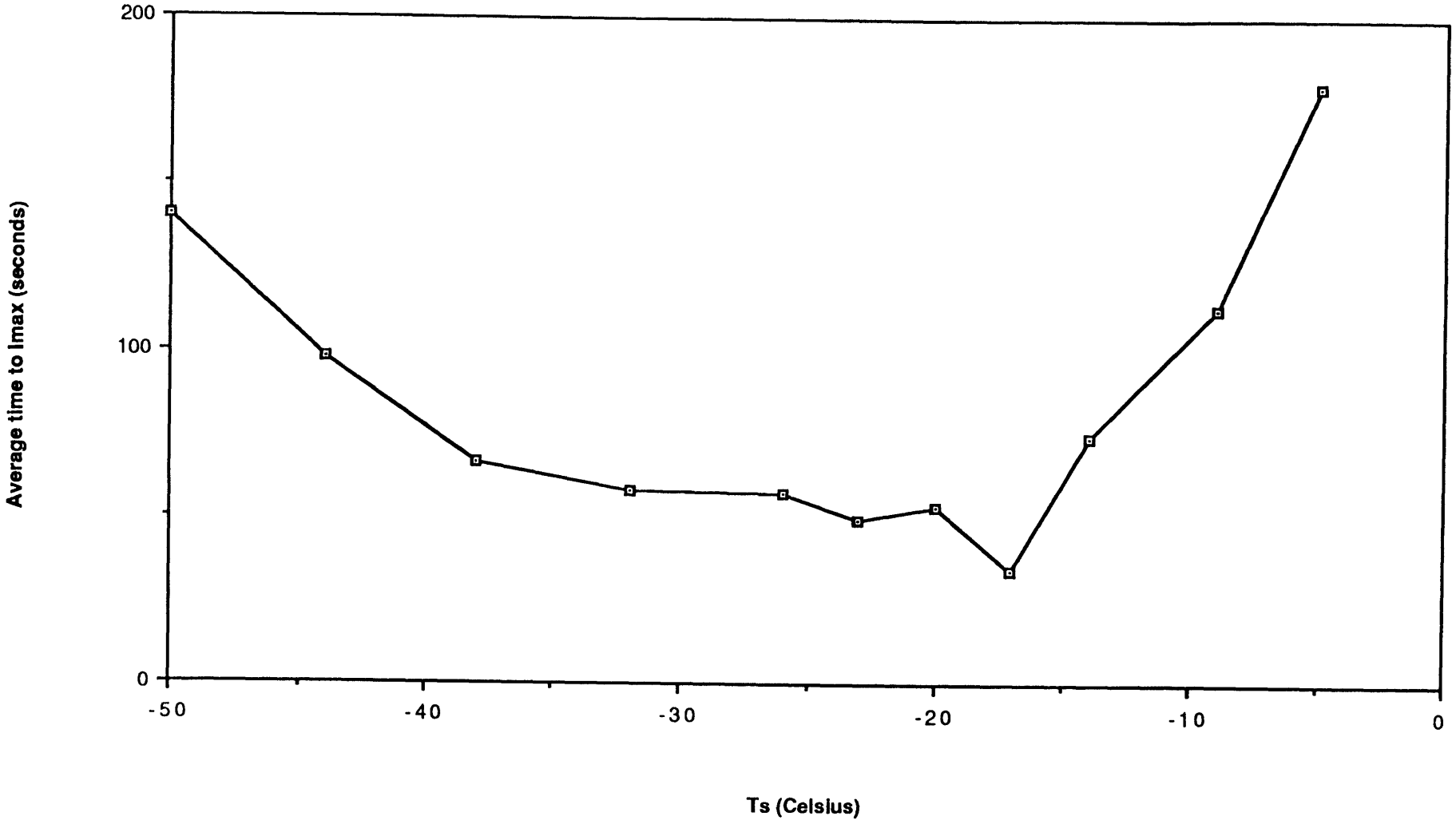

Figure 4A - Average time to I_{max} vs. T_s for runs at T_c=41°C, RH_s=88%.

-50°C and -5°C listed in Table 1. It is assumed that each profile represents the warming behavior of the sphere from the respective T_S, so that we can use this data to estimate an average temperature at the bottom of the sphere at I_{max} for a particular T_S, $\bar{T}_{bimax}$.

To demonstrate the repeatability of these temperature profiles, we present three warmup traces from T_C=41°C, T_S=-20°C, RH_S=88%, in Figure 5. These plots are obtained as follows: The thermistor-amplifier circuit outputs a voltage which is proportional to the resisance of the thermistor (see Appendix A). Values from the voltage vs. time trace are then taken at 1 minute intervals and converted into numbers for electrical resistance . The conversion table from resistance to temperature for the Omega 44033 lists temperatures at increments of °C with a corresponding resistance at each temperature. Thus, to convert our experimental resistances to temperature, we employ a cubic spline algorithm to interpolate between the table-supplied numbers.

Looking at the plots in Fig. 5, we see that for the duration of the runs, at any one time, the T_{bottom} values are always within .5°C of each other. Hence, we are confident that the single profiles obtained for each set of run conditions are a good representation of the temperature history of the non-thermistored, current measurement trials.

The value at $t=\bar{t}_{imax}$ on the temperature profile from the thermistor-amplifier at a particular T_S then yields $\bar{T}_{bimax}$. We stress again that this is the temperature at one location on the sphere, at a knob soldered to the

Figure 5 - Tbottom vs. time for 3 STS runs,Tc=41,Ts=28,RHs=88%

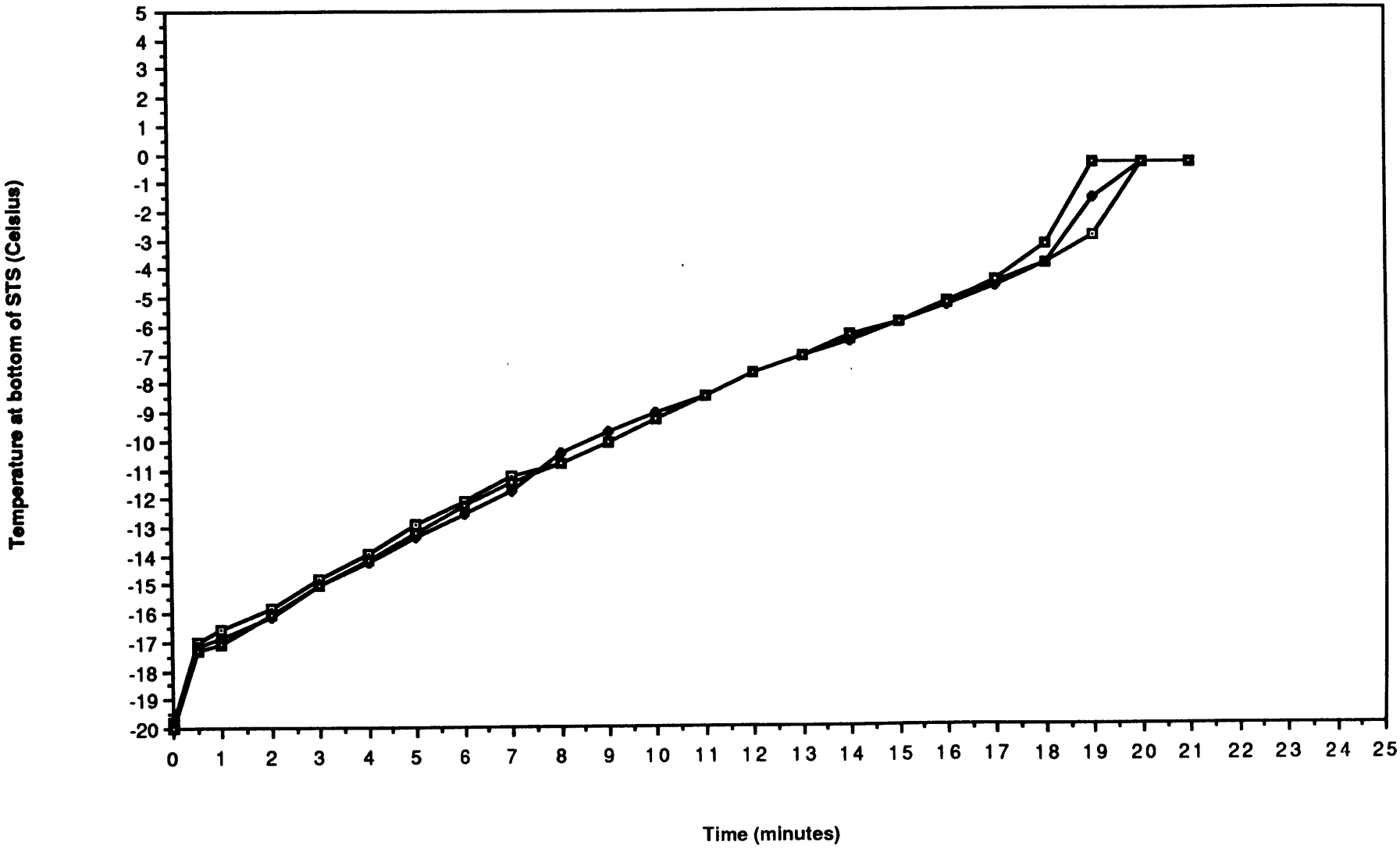

bottom pole of the sphere, at the averaged time to maximum current in the frost growth peak for runs at one freezer starting temperature. This measurement is as accurate a determination of the temperature at the base of the ice growth as is possible with the available equipment. However, the bottom of the specimen is relatively insulated by the cold boundary layer, and hence, a question arises as to the validity of this area as a representation of the entire surface of the object during growth in the warm environment of the experiment chamber.

To examine this question, we mount STS with the two thermistors, one at the bottom and one on the equatorial knob, and compare the warmup profiles from the two sites. The run is done at T_C=41°C, RH_S=88%, T_S=-17°C. The plot of both temperatures vs. time is shown in Fig. 6. The zero of time is the time at which the electronics are turned on after the sphere has been placed in the chamber. The temperature plotted 20 seconds to the left of time zero is the temperature of STS in the freezer. Also plotted in the figure, with the dashed line, is a typical current trace from a run with those initial conditions.

In this data we see a substantial difference in temperature (4-7°C) between the bottom knob and the side knob. Though the side knob is probably slightly warmer than the stainless steel surface at the equator, the sphere clearly does not warmup uniformly across its surface area, and thus T_{bottom} is not a good representation of the temperature at other points on STS during warmup in these run conditions. However, we will see in the next section that the ice crystal ejection activity appears to be

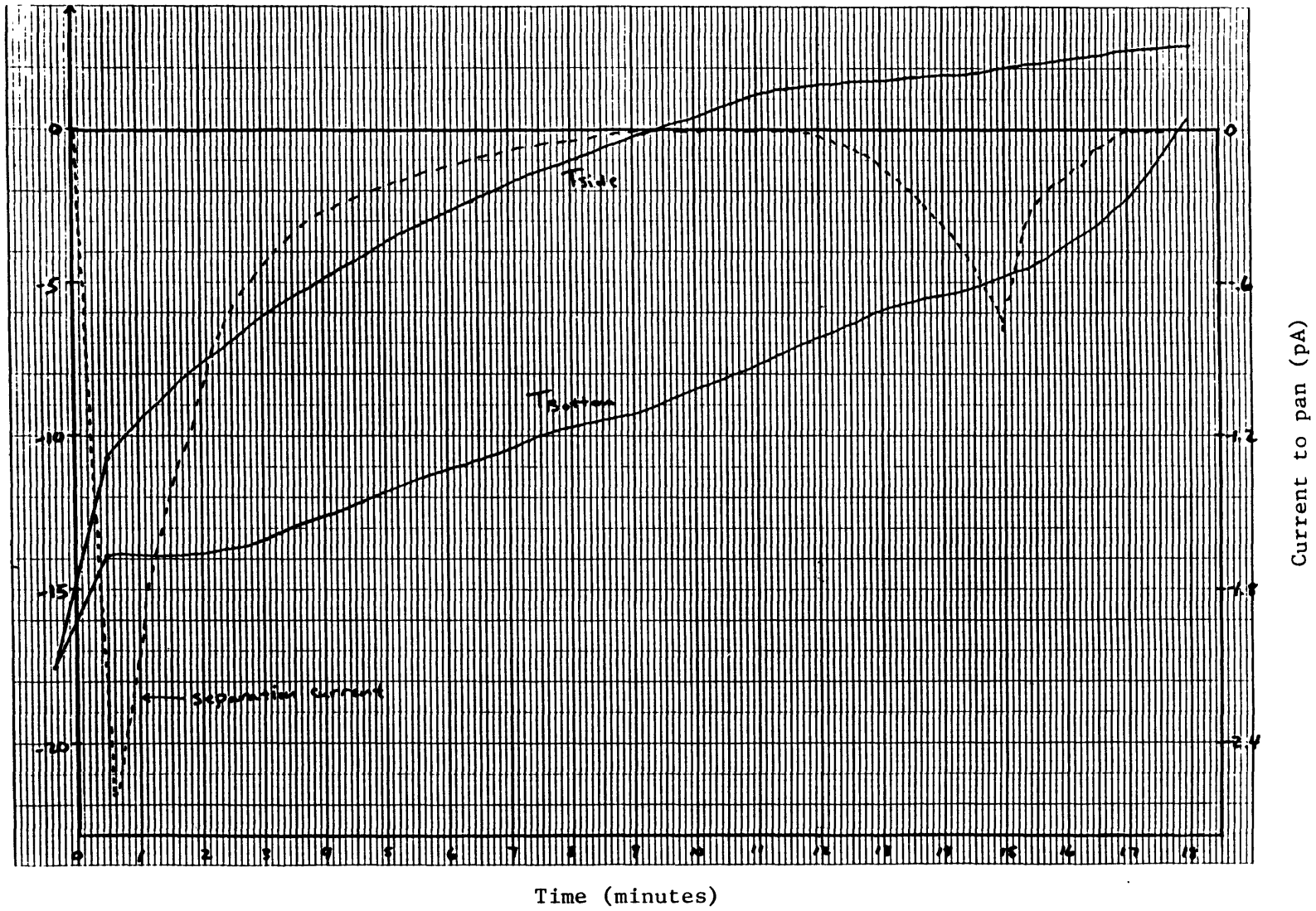

Figure 6 - Temperature at bottom and temperature at side of STS vs. time for a run at Ts=-17°C, Tc=41°C, RHs=88%. Also shown is a typical current trace for a run at those conditions.

confined to a small region including the bottom of the sphere, so T_{bottom} probably is a valid indicator of the temperature at which charge separation is occurring

Returning to Table 1, we see that the $\bar{T}_{bimax}$ values are listed for all eleven specimen starting temperatures. The value in the table is rounded to the nearest degree C. Generally, $\bar{T}_{bimax}$ is increased by about 4°C relative to the initial sphere temperature, T_S. The broad range of $\bar{T}_{bimax}$ is evidence that the current maximum is not simply the result of a growth independent phenomenon occurring at a unique 'resonance' temperature, as the frost growing on the simulated graupel particle warms through this temperature. The charging phenomena appears to depend on the history of frost growth.

To more clearly illustrate this important point we have $\bar{I}$ vs. T_{bottom} plotted for a range of T_S values at T_C=41°C, RH_S=88% in Figure 7. $\bar{I}$ is just the average of the currents from three independent measurements at a particular time=t for the runs at that T_S. To determine the abscissae, we just take the T_{bottom} value at time=t from the temperature vs. time trace at that T_S, T_C, & RH_S (eg. Fig. 6). For each T_S trace shown in Fig. 7, the leftmost point is just the specimen starting temperature in the freezer and is assumed to have a current transfer of 0 pA.

The total charge transferred from the specimen to the pie pan electrode during the frost growth peak can be determined by enlarging the Rustrak traces and using a simple graph paper square counting technique to

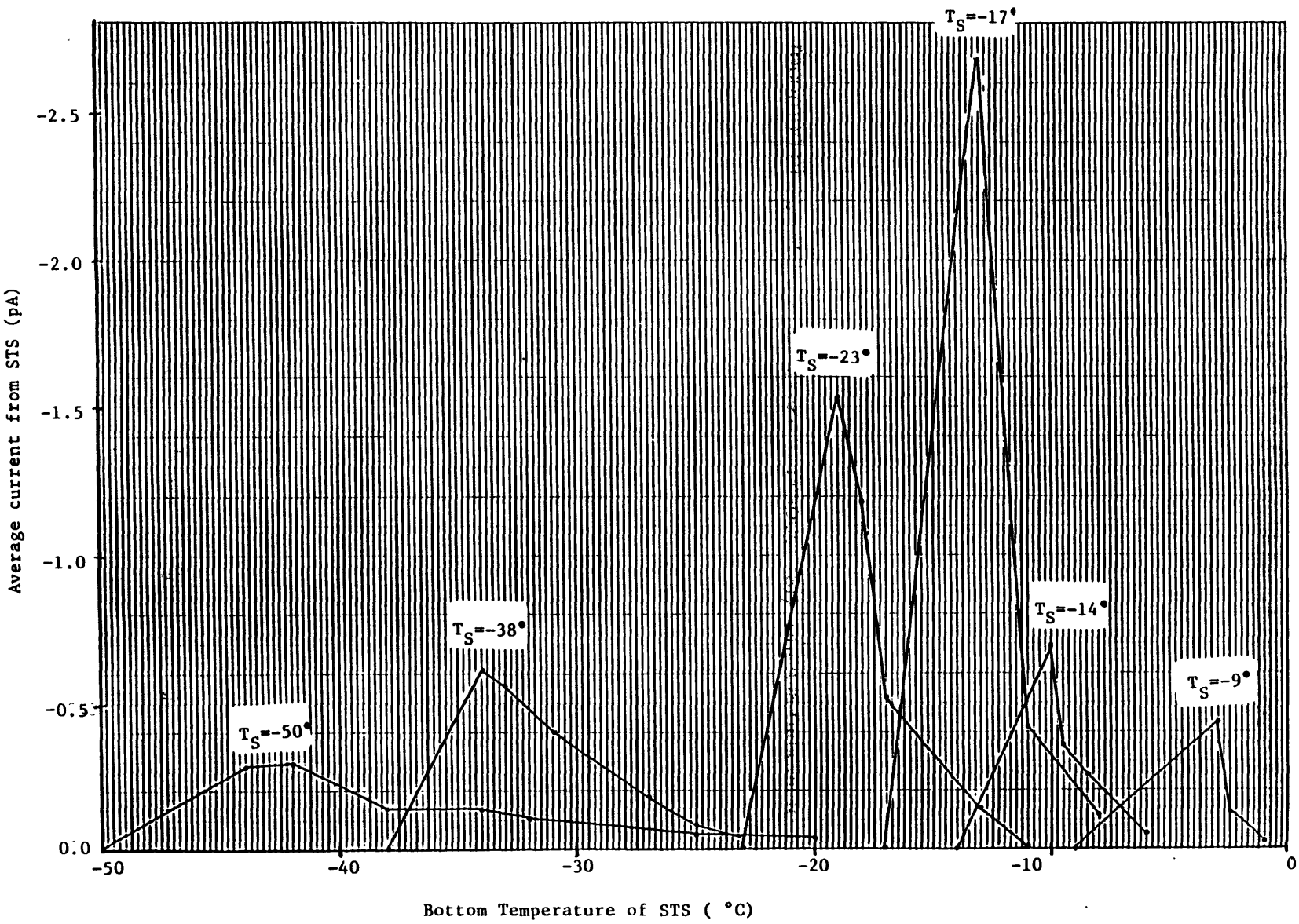

Figure 7 - Average current from STS vs. bottom temperature for selected Ts runs at Tc=41°C.

integrate the area under the current vs. time curve (assuming a continuum process). Table 2 lists some values from the above data at T_C = 41°C. The table is not comprehensive because not all of the Rustrak data is amenable to this technique due to early calibration problems of the chart recorder. Though limited, it is useful. The spread in Q values is much smaller than that in I_{max}. In fact, the total charge transferred in runs at this chamber environment is fairly constant below -17°C, certainly with respect to the factor of five difference across T_S in maximum current values (See Fig. 4).

Next we present the data from experiments done using STS with the chamber temperature at 28°C, RH_S=93%, which has a vapor content (26 gm/m^3) about one-half of the value in the environment at T_C=41°C (50 gm/m^3). The I_{max} vs. T_S results for this less extensive set of runs are plotted in Figure 8. Peak values of the maximum current occur around T_S=-20°C, about a factor of 7 greater than the numbers at T_S=-50°C, which are close to -.2 pA. The plot has the familiar trend seen in STS data at T_C=41°C, with a current cut-off temperature between -3°C and -4°C. $\bar{t}_{imax}$ and $\bar{T}_{bimax}$ numbers are shown for 10 values of T_S in Table 3. $\bar{t}_{imax}$ vs. T_S is also plotted in Figure 8A. The average times to maximum current are considerably longer than for runs with STS at T_C=41°C, and again the shortest $\bar{t}_{imax}$ of 84 seconds is at the temperature with the highest I_{imax}, T_S=-20°C. Note also that $\bar{T}_{bimax}$ at this can temperature is

Table 2 - Total charge transferred (Q) for STS, T_C=41°C

T_S (°C)	Q (pC)	$Q_{average}$ (pA)
-50	-310	-310
	-300	
-44	-200	-200
-38	-210	-210
-32	-220	-220
-26	-250	-250
-20	-290	-340
	-360	
	-380	
-17	-290	-290
-14	-150	-110
	-64	
-9	-40	-52
	-64	

Figure 8 - Data from STS, Tc=28 C, RHs=93%

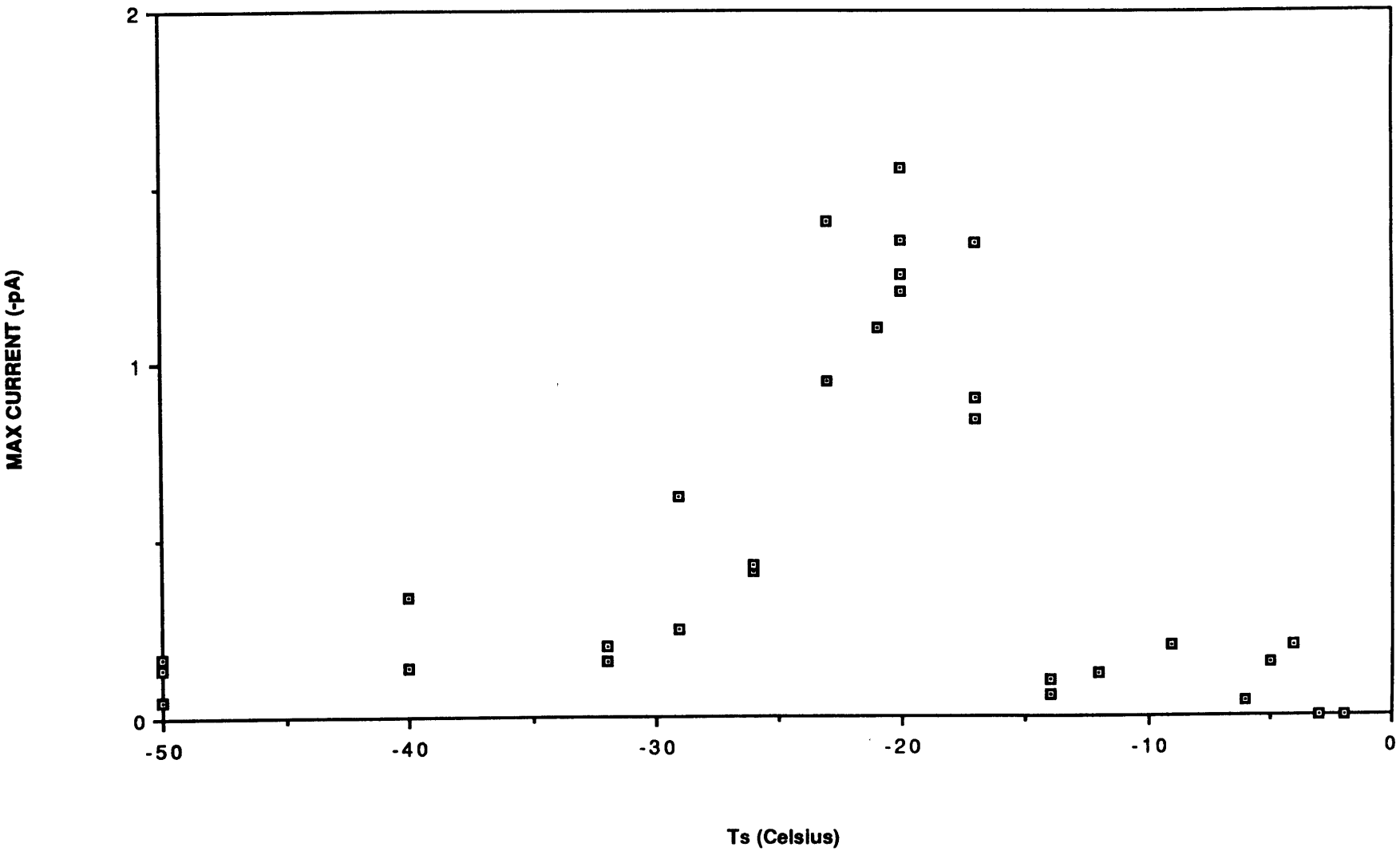

Table 3 - Time ($\bar{t}_{imax}$) and temperature ($\bar{T}_{bimax}$) at the bottom of STS at I_{max}, T_C=28°C, RH_S= 93%

T_S (°C)	t_{imax} (sec)	T_{bimax} (°C)	I_{max} (pA)
-50	213	-45	.13
-40	265	-34	.24
-32	211	-29	.19
-26	112	-23	.42
-23	84	-21	1.18
-20	76	-18	1.34 *
-17	87	-13	1.03
-14	197	-9	.08
-9	170	-6	.20
-4	330	-1	.21

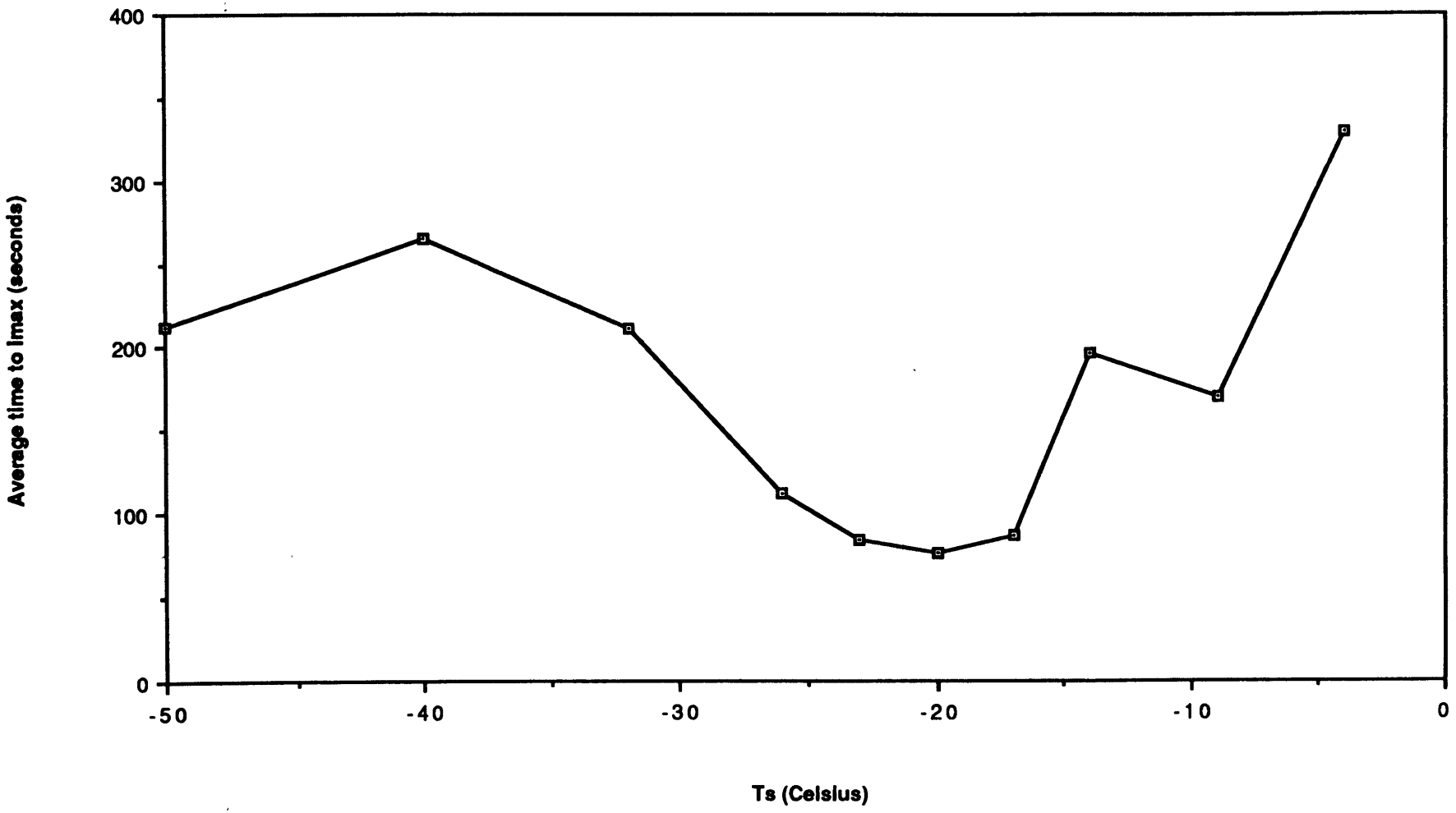

Figure 8A - Average time to I_{max} vs. T_s for runs at T_c=28°C, RH_s=93%.

not the same as the value for T_C=41°C, being about 5°C colder at T_C=28°C than the $\overline{T}_{bimax}$ number of -13°C for the warmer chamber environment.

The third and smallest set of STS data is taken at T_C=52°C, RH_S=84%, a chamber environment with approximately 1.5 times the vapor content of the T_C=41°C runs. The I_{max} vs. T_S plot for these trials, shown in Figure 9, exhibits much more erratic behavior than the numbers for STS at the lower drum temperatures. Still, the trend of increasing I_{max} with increasing T_S from -50°C is evident. Maximum currents of -12.0 pA and -10.5 pA are recorded at T_S=-21°C and T_S=-23°C respectively, but it is difficult to discern confidently a peak response temperature in these data due to the substantial variance in the measurements. Note that the above two I_{max} values are approximately 4 times greater than the largest numbers at T_C=41°C, RH_S=88%. Response times ($\overline{t}_{imax}$) are significantly faster than for runs with T_C=41°C, ranging from about 1 minute for T_S=-50°C down to around 10-15 seconds for the maxima just below T_S=-2 °C. Such times are dangerously close to the response speed of the ammeter. Perhaps this is a contributing factor to the large variance in the I_{max} values at this high can temperature. No sphere warmup temperatures were monitored during this set of trials.

To demonstrate that there are characteristics of the charge separation phenomena that appear to be indepedent of metal type used, we next consider data taken with the aluminum specimens as simulated

Figure 9 - Data from STS, Tc=52 C, RHs=84%

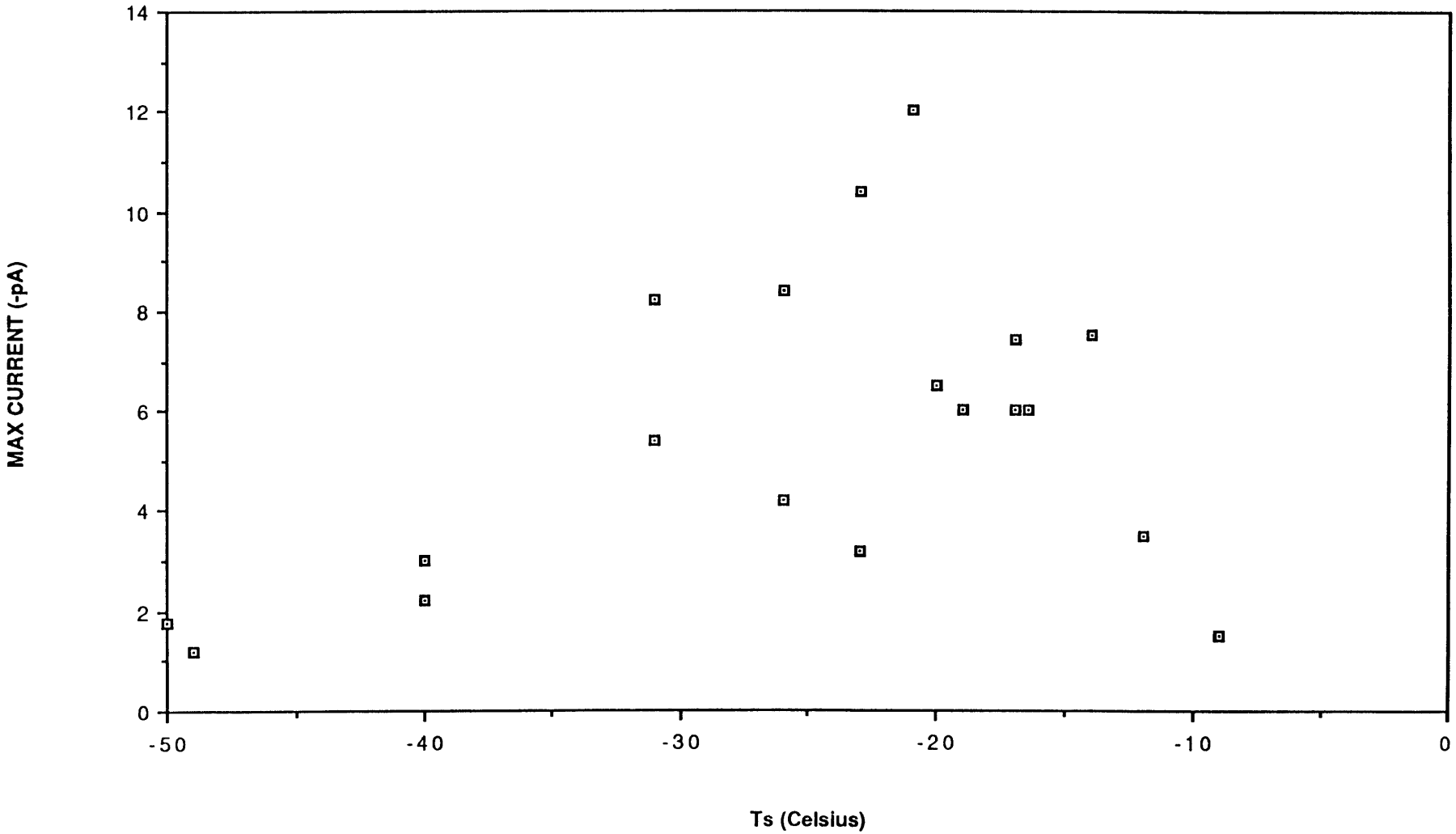

hydrometeors. We have found that the aluminum electrodes yield results with a greater variance than runs with STS. This is consistent with reports in the literature that aluminum is perhaps questionable for use as an electrode (Sill, 1963). Because of this we place less emphasis on analysis of the aluminum data.

First we present I_{max} vs. T_S plots for the two aluminum cups, designated AL1 and AL2, at T_C=41°C, RH_S=88%, in Figures 10 & 11. These results show systematic differences in the responses of the two cold objects in several temperature regimes and thus we have kept this data separate and do not consider the two specimens interchangeable. The tinting of the two hemispheres is slightly different, but the supplier claims that the manufacturing process and metal used has not changed to their knowledge. Perhaps the older cup, AL1, has become oxidized.

For both AL1 and AL2 there is similarity with STS in that I_{max} increases with increasing T_S from -50°C, though the variance in the values at any one freezer starting temperature is greater. Figure 10 suggests a maximum in I_{max} for AL1 near T_S = -32°C, with a systematic decrease at higher temperatures to a current cut-off value between -14°C and -9°C (Again, T_S is the temperature at the equator of a hemisphere just before it is pulled from the freezer for a run). The latter behavior is also followed by AL2. As was the case for the STS cutoff temperature, this seems to be the regime in which frost never forms on the cup surface, just condensation. The much lower cutoff temperature for the aluminum

Figure 10 - Data from AL1, Tc=41 C, RHs=88%

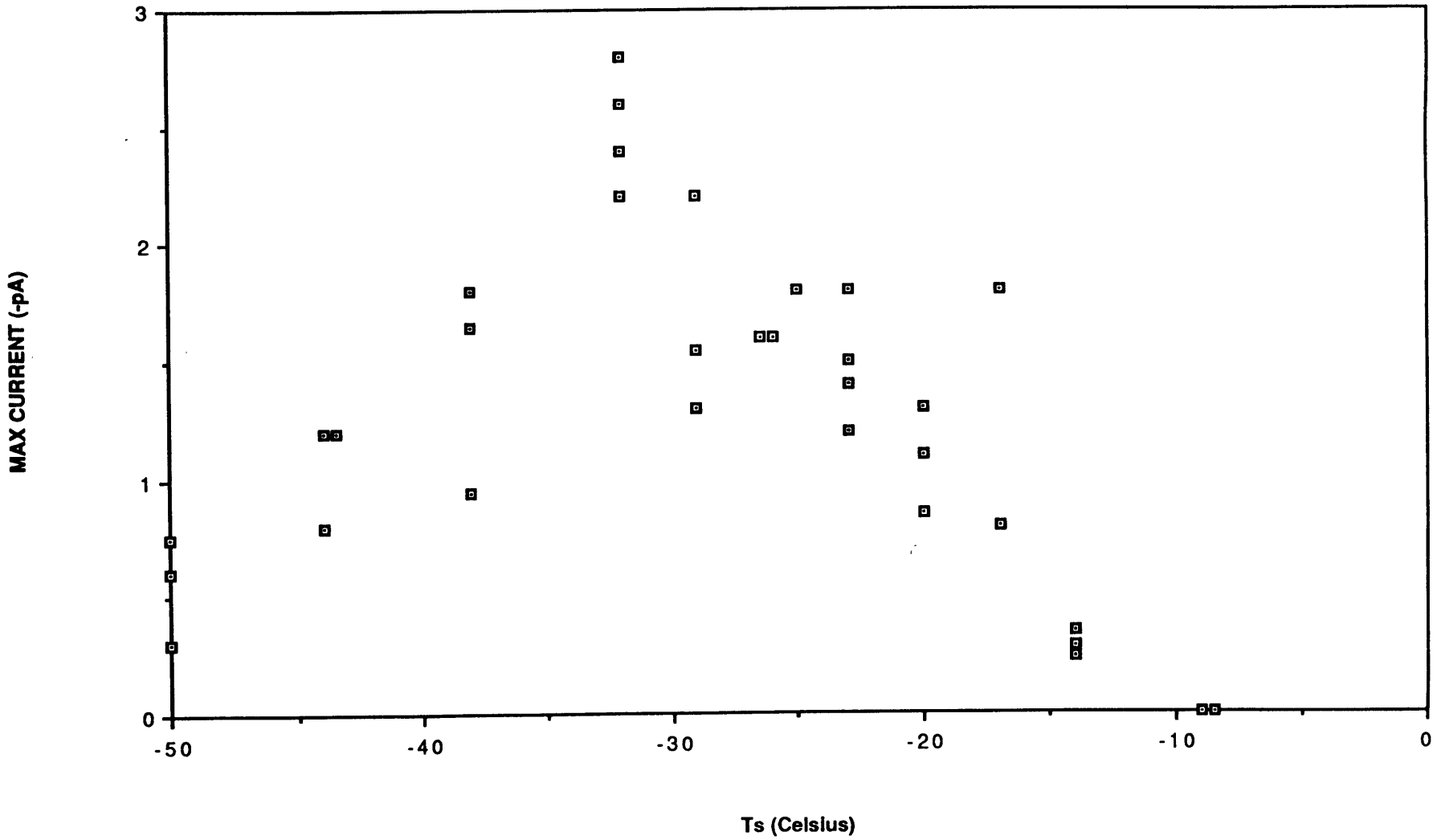

Figure 11 - Data from AL2, Tc=41 C, RHs=88%

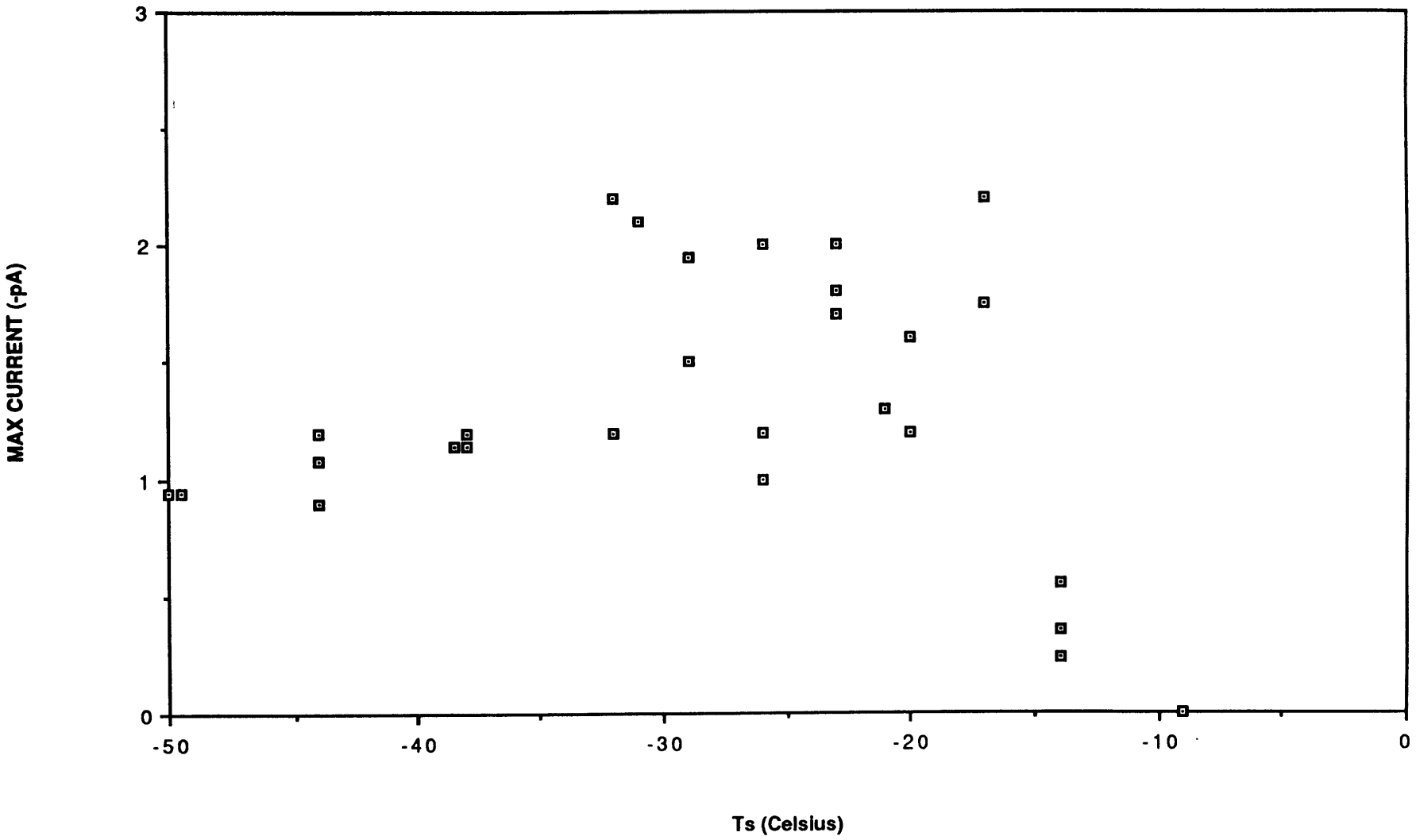

cups is most certainly a result of a geometry-dependent difference in warmup behavior. In Figure 11, the position of the maximum is less well defined, lying somewhere between T_S = -32°C and T_S =-17°C.

The I_{max} magnitudes for AL1 & AL2 at T_C=41°C are similar to STS. Direct comparisons at specific T_S values are not meaningful, again, because the two geometries exhibit substantially different warmup profiles. Total run times at T_C = 41°C range from about 25 minutes at T_S =-50°C to about 7 minutes at T_S =-14°C. $\overline{T}_{bimax}$ for the aluminum cups is about 9°C warmer than T_S in this growth environment, yielding a value of -23°C for the -32°C I_{max} value for AL1. The value of I_{max} for AL2 lies in the -23°C to -8°C range; the large variance in the measurements may obscure the more narrowly defined peak for STS (Fig. 4). The reasons for the greater variance in the measurements with the aluminum cups is still not understood.

The current vs. time profiles prior to melting for the aluminum hemispheres are generally indistinguishable from STS profiles of a similar magnitude and T_S regime. In other words, the risetimes and Q values for AL1 and AL2 at T_C = 41°C are about the same as for STS. An example to illustrate this is shown in Fig. 12. The -2.25 pA peak in fig 12a) is from an STS trial at T_S=-20°C, T_C=41°C, with a total charge separation (Q) of 360 pC and a risetime of 55 seconds. The trace in Fig. 12b) is from one of the runs with AL1 at T_S=-32°C, T_C=41°C, which yielded a maximum current of

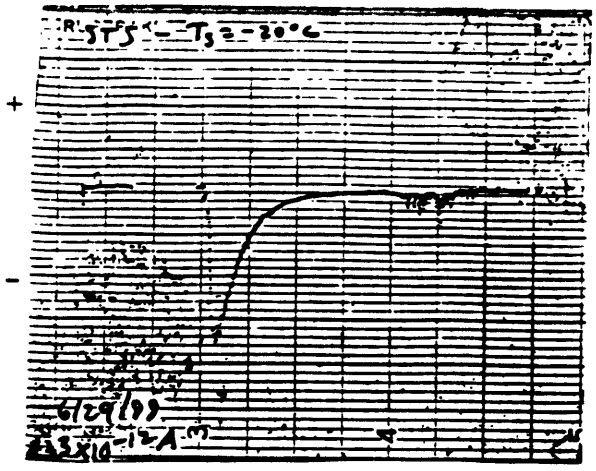

(a)

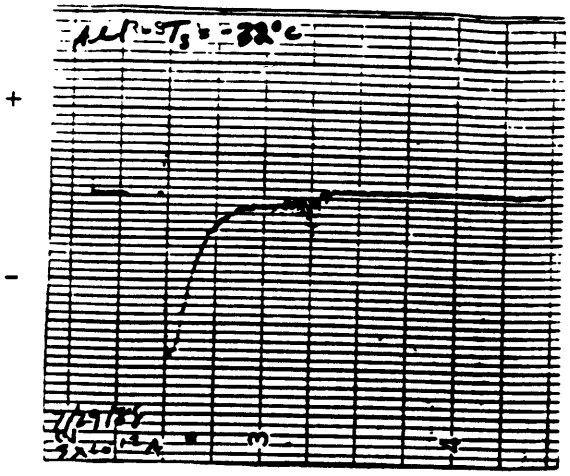

(b)

Figure 12 - (a) current trace from STS trial at Ts=-20°C, Tc=41°C, RHs=88%, full scale = 3 pA, & (b) current trace from ALl trial at Ts=-32°C, Tc=41°C, RHs=88%, full scale = 3 pA.

-2.4 pA and Q=370 pC, with a risetime of about 40 seconds.

As has been previously discussed, the current peak during frost growth and the melting spike are the standard signatures for runs done with the metal simulated hydrometeors. However, trials at -44°C and -50°C, especially with the aluminum hemispheres at T_C = 41°C are an exception to this rule. An example is shown in Figure 13. This run shows what appears to be two current peaks associated with frost growth. Also, for the spheres at these lowest temperatures studied, the initial current peak often decays in what appears to be a departure from the exponential behavior, and occassionally a second peak at T_S=-50°C appears (For example, see Appendix C). This effect shall be discussed further in the Interpretation section.

As was the case with STS, the data with the aluminum hemispheres at T_C=28°C is less extensive than at T_C=41°C. I_{max} vs. T_S at T_C=28°C, RH_S=93% for AL1 and AL2 are shown in Figures 14 & 15 respectively. The profile for AL1 at this temperature is similar to that with the same cup at T_C=41°C, but the maximum appears to be shifted to the right a few degrees Celsius, to around -29°C. $\overline{T}_{bimax}$ for T_S=-29°C is -23°C, which is the same value of the bottom temperature at the average time of maximum current for the -32°C peak in the AL1 data at T_C=41°C. The AL2 data at T_C=28°C do not exhibit a narrow maximum, as was the case for runs at T_C=41°C, but points between T_S=-30°C and T_S=-20°C are clearly greater than the I_{max}

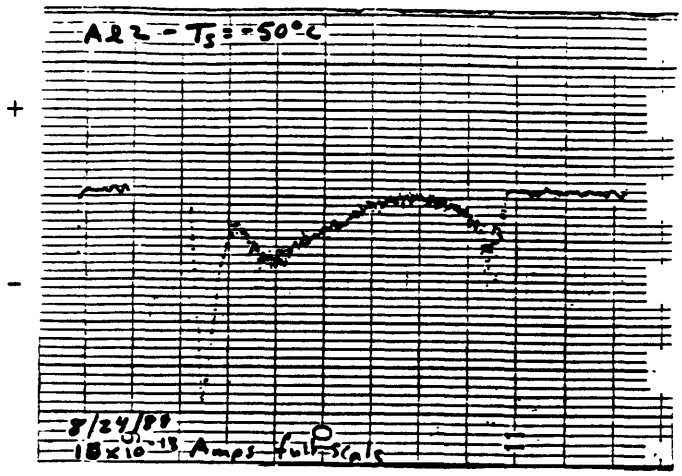

Figure 13 - Current trace from AL2 at Ts=-50°C, Tc=41°C, RHs=88%, showing example of double peak. Full scale is 1 pA.

Figure 14 - Data from AL1, Tc=28 C, RHs=93%

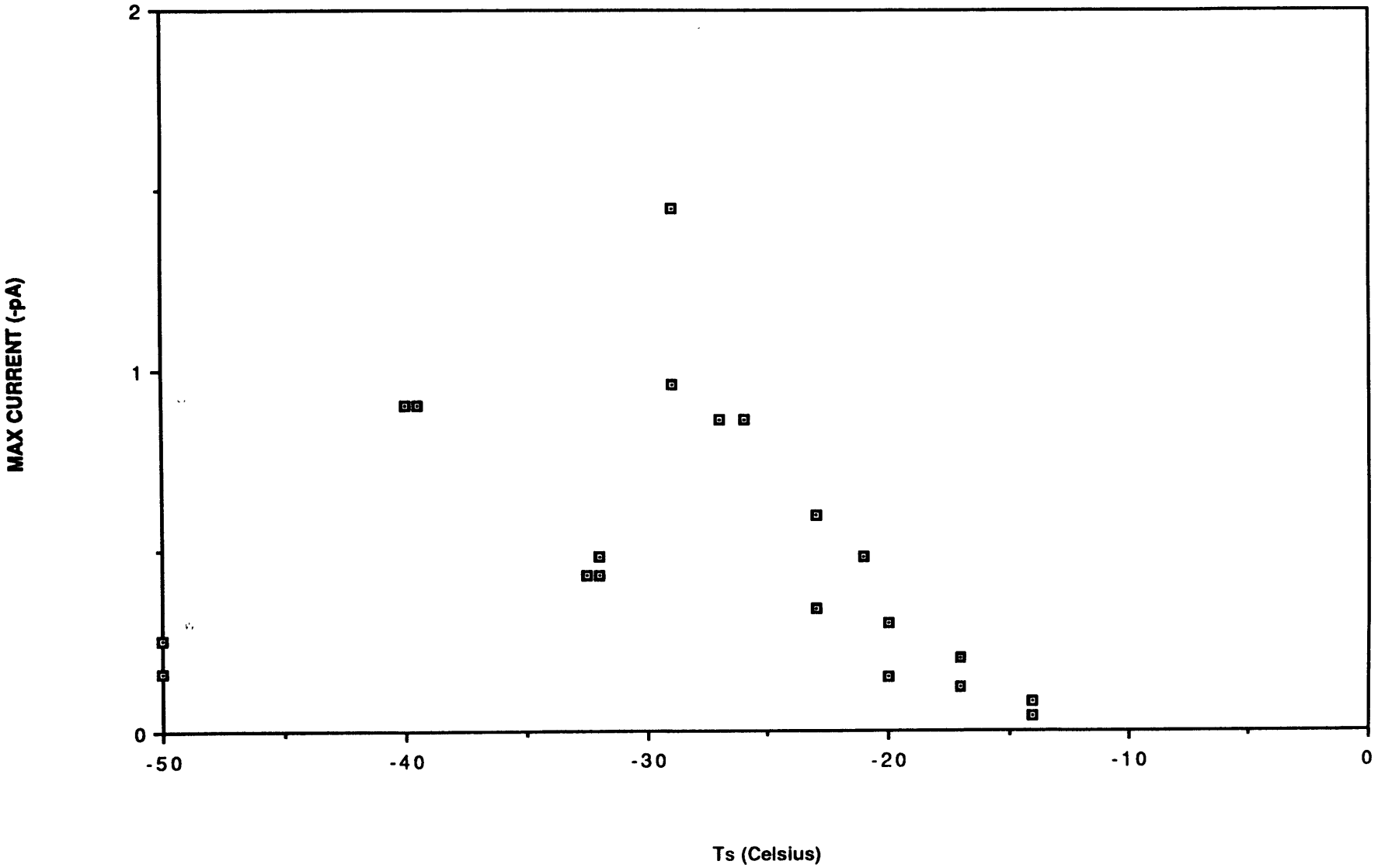

Figure 15 - Data from AL2, Tc=28 C, RHs=93%

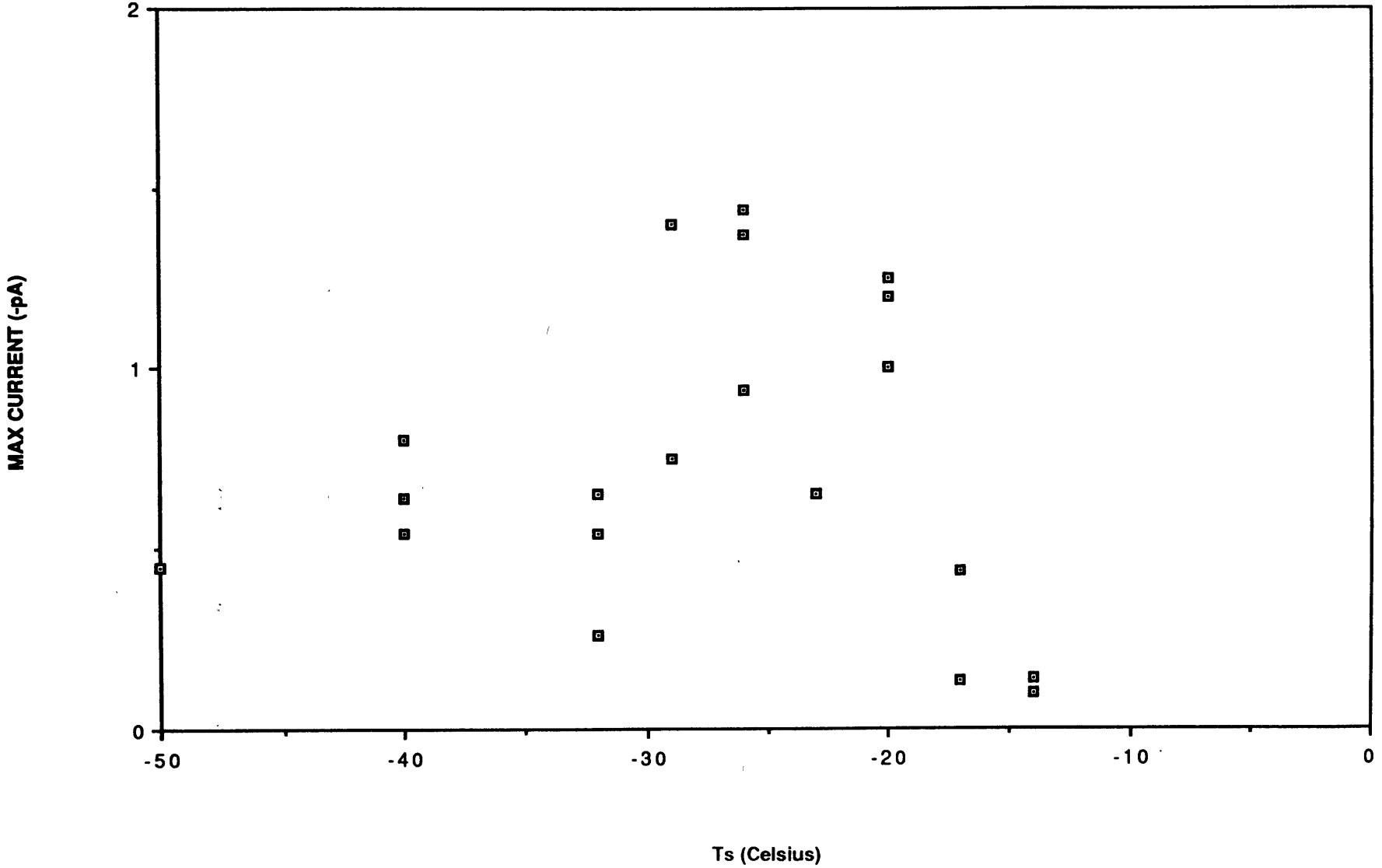

numbers on either side. $\bar{T}_{bimax}$ for T_s=-20°C for AL2 here is -15°C. Maximum I_{max} currents in Figures 14 & 15 are about -1.4 pA, roughly half of the peak values seen in the aluminum hemisphere trials at T=41°C.

The I_{max} data for the 6" diameter aluminum sphere (ALS) at T_c=41°C, plotted vs. T_s in Figure 16, is even more erratic than the AL1 & AL2 results. Again, though, it is clear that the maximum current value broadly increases with decreasing T_s up to about -25°C and then decreases to nearly zero by -4°C. To be more specific is difficult in light of the large variance in these results. It is interesting to note that the highest currents recorded, nearly -2.0 pA at T_s =-26°C, are smaller than the largest I_{max} values of AL1 & AL2, which have smaller surface areas than the sphere. There is no $\bar{T}_{bimax}$ data for ALS, but the total run times agree closely with those of STS (also 6" diameter) at the same freezer starting temperatures, so the warmup profiles are probably similar. Also, as with the aluminum cups, current peaks associated with frost growth for ALS are indistinguishable from current peaks for STS of the same magnitude.

The last set of data to be discussed are the runs with the ice hemispheres at T_c=41°C. In earlier experiments it was determined that results using Cambridge tap water ice are indistinguishable from distilled water ice trials. Distilled water is used only because it has a constant, known composition and is probably more representative of the composition of ice particles in the atmosphere. Though ice is a poorer thermal conductor than metal and the specimens are not grounded during runs, the

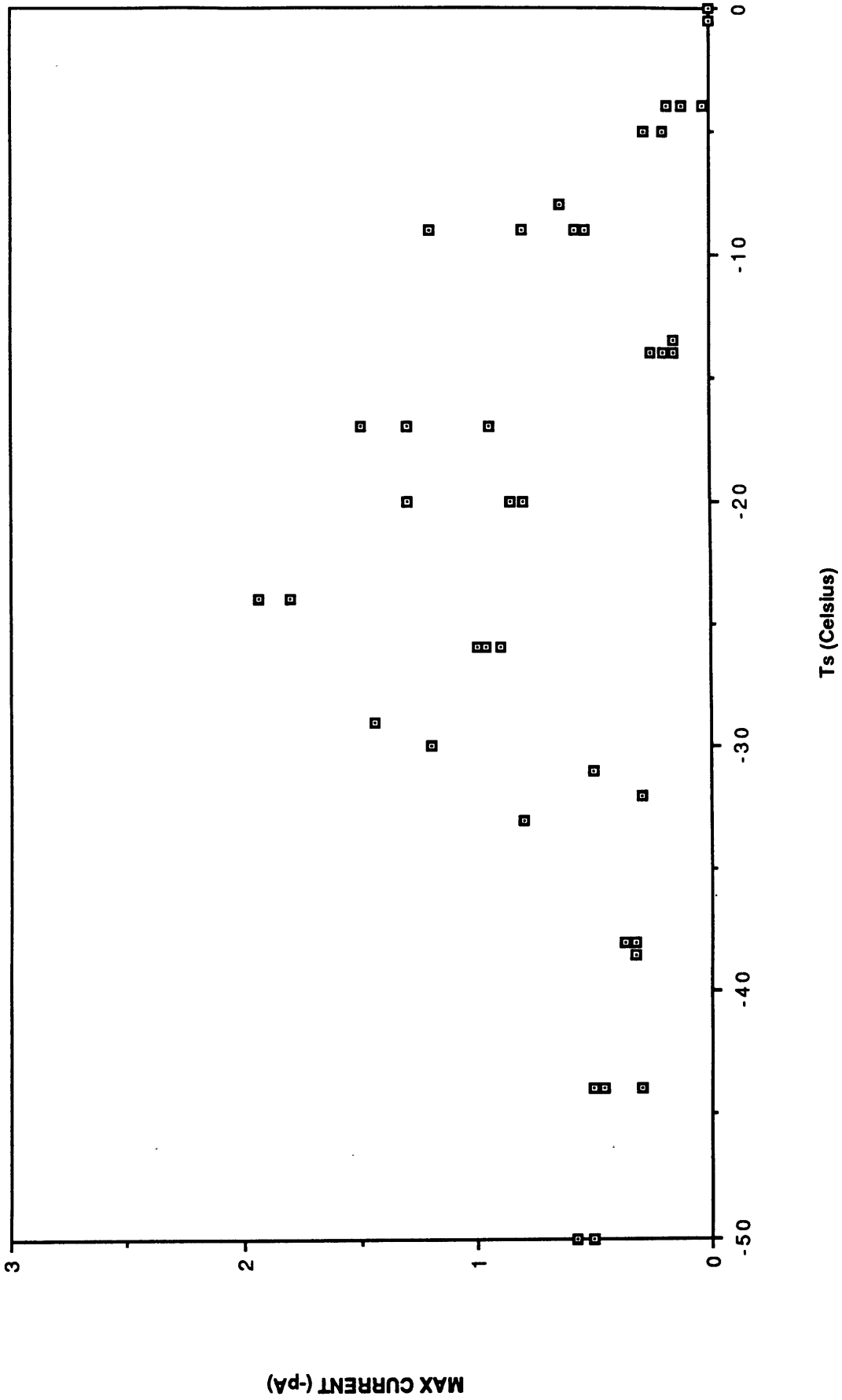

Figure 16 - Data from ALS, Tc=41 C, RHs=88%

results do show similarities with the data for the metallic simulated hydrometeors. An early current peak is a persistent feature. However, systematically at T_S=-24°C, and several times at other freezer starting temperatures, the current trace has a positive excursion in the first 10 seconds or so of the run and then reverses to the normal negative transfer to the plate. An example of this is shown in Figure 17. This sign change is generally difficult to discern because it occurs so quickly into a run that it is often unclear whether the signal is just the result of the settling down of the picoammeter after the cold object is placed in the chamber. However, the case in Figure 17, which is representative of T_S=-24°C for the ice hemisphere runs, cannot be dismissed as an instrument response effect. The amplitude of the positive excursion fluctuates greatly from run to run, sometimes going off the scale at the particular ammeter setting for the experiment. The limitations imposed by the initial boundary conditions make this phenomenon very difficult to quantify.

The I_{max} vs. T_S plot for the distilled water ice hemispheres at T_C=41°C (See Fig. 18) does show an increase in I_{max} as T_S increases from -50°C that is not inconsistent with the metal data. The diamond data points are cases with a clearly discernible initial positive current deviation to the pan. The values shown are the maximum negative currents to the pan during the frost growth phase of a run. Obviously, the figure is not very useful as it stands. The variance in these measurements is even greater than the results for the aluminum cups in Figs. 10 & 11. We feel that the inconsistencies evident in this data are a direct result of the inability to

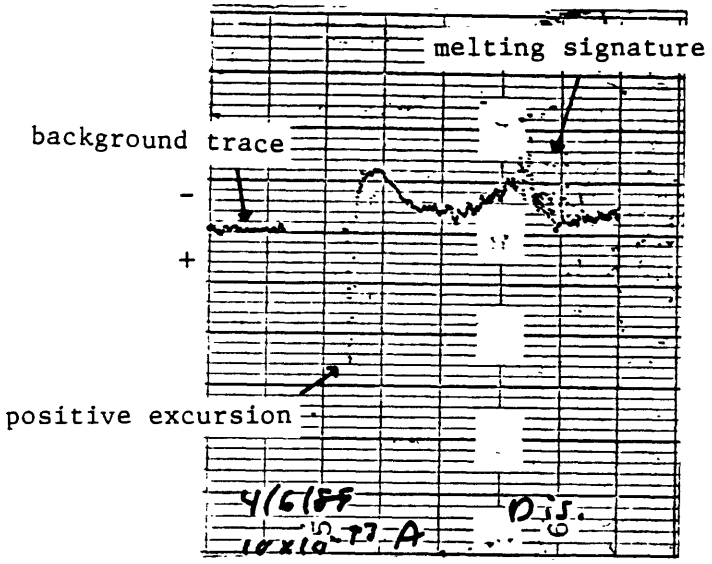

Figure 17 - Current trace for run with water ice cup at Ts=-24°C, Tc=41°C, RHs=88%, showing positive excursion in peak associated with frost growth.

Figure 18 - Data from ice 'cups', Tc=41 C, RHs=88%

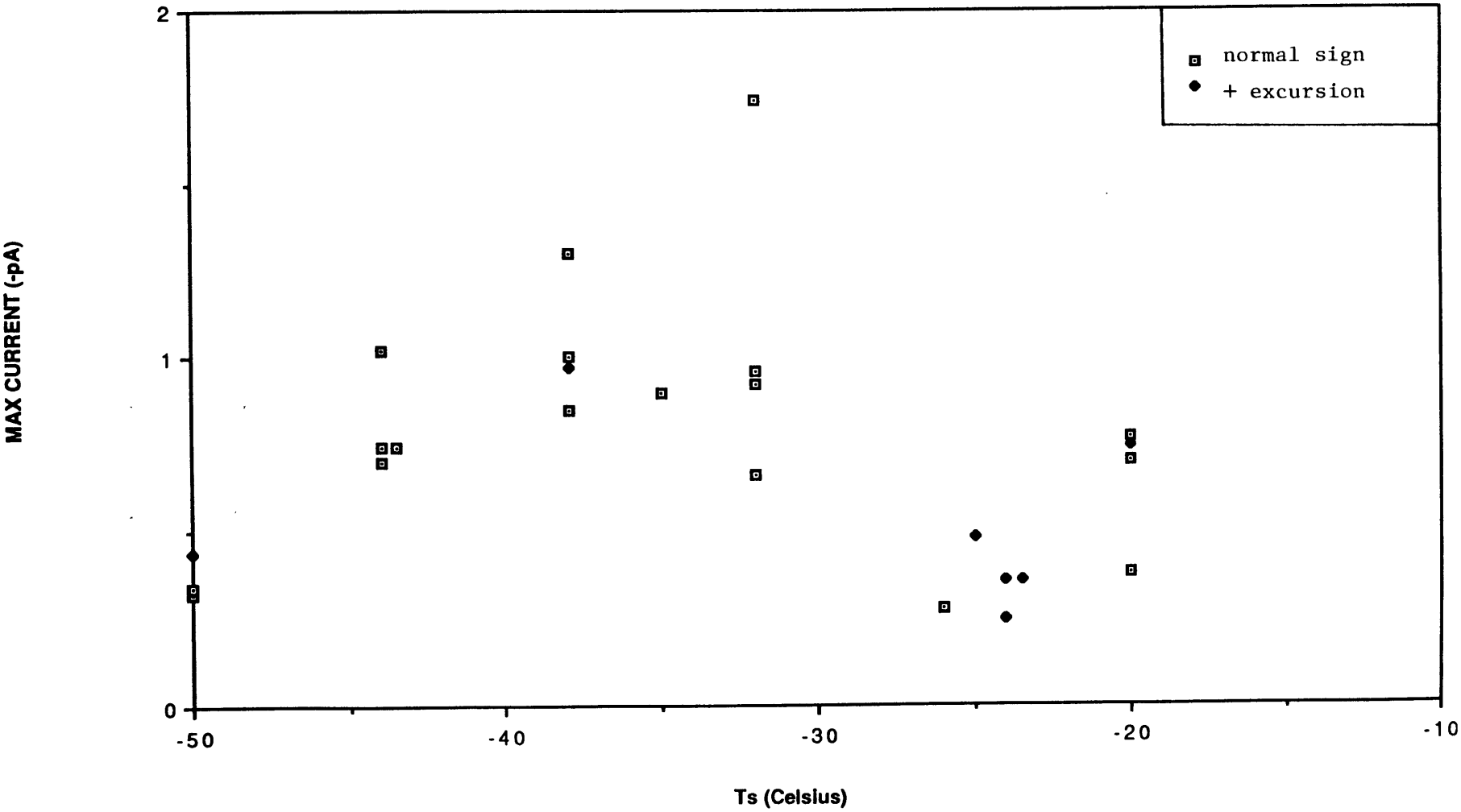

monitor the ice temperature and to be certain of the surface state of the ice at the beginning of a run. For example, a slight temperature disequilibrium with the freezer air, which is most surely present in a thermostat controlled freezer, can put the surface alternately in a state of evaporation or deposition, with consequent electrical effects. This is easy to identify and control on a metal surface, but not so with an ice surface. This, combined with the uncertainty in the initial boundary condition makes further analysis of the distilled water ice data unrewarding.

Before proceeding to the next section, we must make some comments about the problem of controlling and determining the relative humidity during a run imposed by the experiment procedure. As was stated in the experiment section, the three temperature/moisture environments were chosen so that the ratio of the total vapor content in the chamber would increase roughly as .5 : 1.0 : 1.5 for the three temperature regimes: 28°C, 41°C, & 52°C. This is assuming, of course, that RH_S is a reasonable representation of the relative humidity in the can during frost growth. However, again, when the drum lid is slid off, mixing occurs with the outside air, to an extent determined by how long the chamber is open, which is relatively constant from run to run (5-10 seconds), and also by the temperature contrast with the surrounding environment. It turns out that the relative humidity during the current peak associated with frost growth for different T_S runs at a particular T_C is fairly constant, usually within ±3%. Figure 19 shows a typical relative humidity vs. time trace for the beginning of a run at each of the three chamber temperatures. On the strip chart, one division horizontally is 30 seconds and 5 divs in the

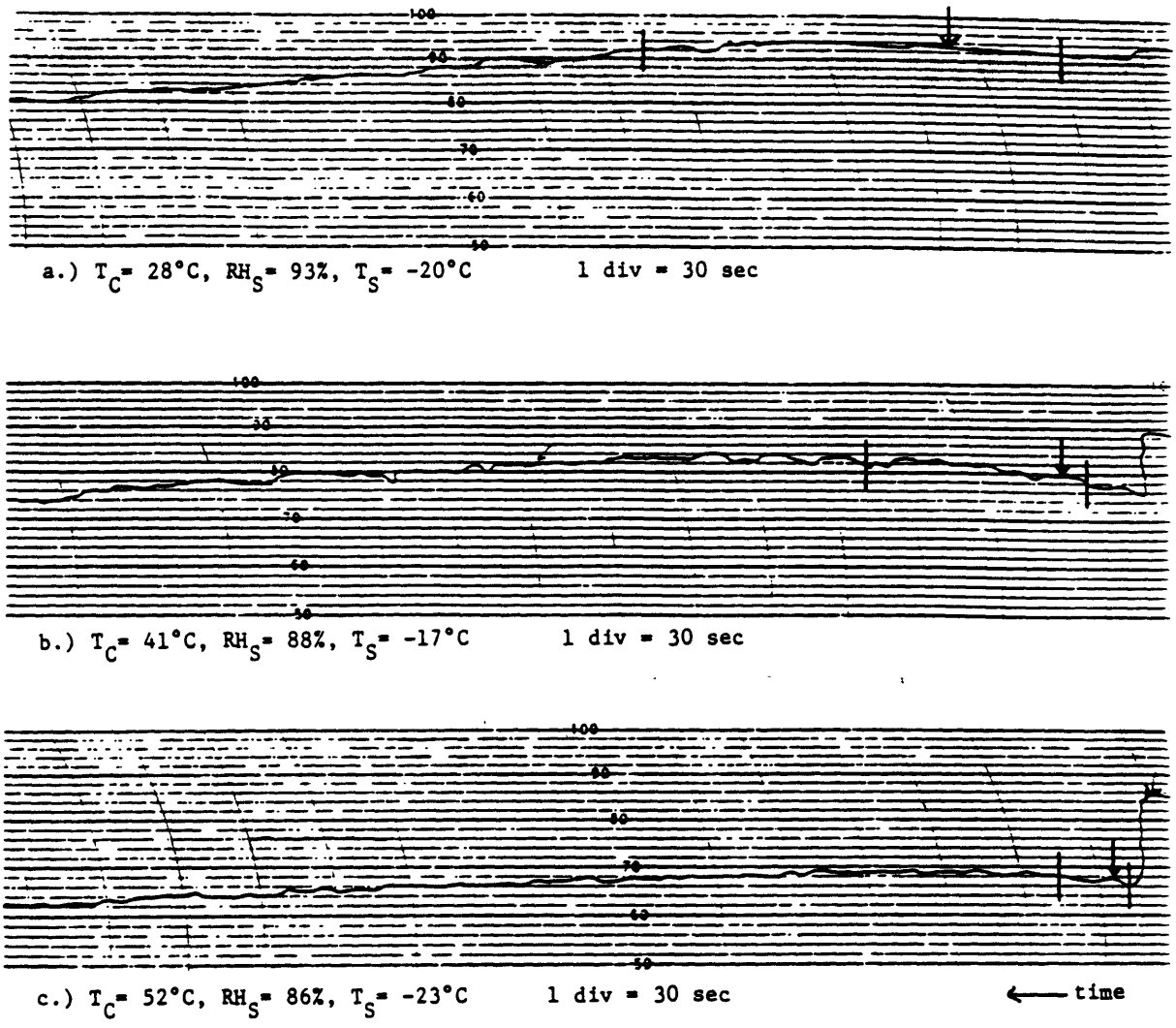

Figure 19 - Three chamber relative humidity vs. time traces with STS, one at each growth environment used in the experiment.

vertical is 10% relative humidity at that T_S. Runs begin at the right hand side with the sudden drop in RH. Fig. 19(a) is a trial at T_C=28°C, T_S=-20°C, RH_S=93%, while 19(b) is done at T_C=41°C, T_S=-17°C, RH_S=88%, and 19(c) has initial conditions of T_C=52°C, T_S=-23°C, RH_S=86%. Note that as T_C increases, the initial drop in relative humidity increases as well, due to the increasing contrast between the air in the can and in the laboratory.

There are some interesting features that are common to all three of these traces. After the initial drop in RH caused by the uncovering of the chamber lid, the relative humidity is seen to rise for several minutes before falling steadily for the remainder of the run. This is undoubtedly due to the proximity of of the humidity sensor to the top of the can. The upper layers of air are mixed most with the laboratory air, and when the chamber is once again closed, convective homogenization with the relatively unmixed air at the bottom causes the apparent rise in relative humidity in the can. After this initial homogenization, the accumulation of ice on the simulated hydrometeor slowly depletes the vapor supply and hence the RH reading begins to fall. This is consistent with measurements of the mass growth on the sphere which will be presented in a later section. For example, the can environment in trace (b)., for the .208 m^3 can, yields a total water content of about 10 g. Our measurements of the 2-minute mass growth in this environment suggest growth accumulations after 5-10 minutes that should be an appreciable fraction of 10 grams, and this should be refelected in the RH trace. Note also in Figure 19 the short term, small amplitude variations in the signal, caused by the point source

(the water pan at the bottom of the chamber) and sink (the simulated hydrometeor) of water vapor in the presence of convective overturning.

Also shown in Fig. 19 for each RH trace is an arrow marking the time of a typical peak at that T_S and lines marking the full width at half maximum (FWHM) for a typical current trace. Of course, the position of I_{max} and the FWHM will vary somewhat across T_S at one T_C, but if we assume the time periods around the FWHM's shown are representative of the times when, generally, most of the charge separation occurs, we see that the average RH for 19a) is about 93%, while for 19b) it is approximately 80%, and for 19c) the average is 68%. These three values yield total vapor contents of 26 gm/m^3, 45 gm/m^3, and 67 gm/m^3 respectively, or a revised ratio of .6 :1.0: 1.5 for the three principal can environments used in the experiments.

Further Observations

In analyzing the data presented above there are obvious and systematic features which we must attempt to account for. Clearly, there is a substantial variation in average maximum current across T_S at any one particular growth chamber environment, and there is also a large variation

in I_{max} at a given T_s across the three principal chamber temperatures. Before addressing these trends, though, we will take a step back to examine information revealed in several supplemental qualitative observations and quantitative measurements performed in an effort to answer more basic and general questions about the phenomenon. For example, Are we sure the charge carriers are, in fact, ejected ice crystals?

The observation window drilled into the wall of the ice growth chamber proves to be a very useful tool for qualitative analysis of the charge separation problem. A typical trial proceeds as follows: At the start of a run, when the cold object is first placed in the drum, it is sheathed in an optically thick supercooled condensation cloud. The condensation boundary layer is relatively thin higher up on the simulated hydrometeor, but near the bottom (perhaps 25 degrees from the bottom) it separates from the surface and forms a cylindrical flow shedding from the lower pole. The observed features of the flow are qualitatively consistent with numerical results for buoyancy induced single phase flows by isothermal spheres (Gebhart,1987). The range of simulated hydrometeor sizeand chamber temperature in our experiments yields Grashof numbers (analogous to the Reynolds numbers of forced flows, See Eqn. 9, p.76) of $1X10^7$ to $5X10^7$ (See Table 4) for these experiments, with corresponding boundary layer thicknesses above the separation point on the order of 5mm (Gebhart, 1987, p.214).

Initially, there are no ice particles discernible in the flow, but as the frost becomes noticeable on the surface of the simulated hydrometeor, a

myriad of tiny ice fragments becomes visible reflecting in the chamber light. It appears that these miniscule particles emanate from the bottom of the sphere or cup, and that the middle and top facing areas are not involved. An example of the view from the observation hole of the ice fragment ejection from the bottom of the stainless steel sphere, with the condensation sheath and associated flow separation, is illustrated in Figure 20.

As the frost growth progresses, chunks of dendritic structures, perhaps 2-3 mm in diameter, are seen falling into the pan along with the tiny splinters. This is most evident in the runs at the lowest freezer starting temperatures. Thick accumulation of frost is maintained on the inactive areas on the top and sides of the cold object, while from a critical angle (about 20° from the bottom) on the lower face down to the bottom pole, it appears the thick frost cannot be mechanically supported. This area is continually shedding large frosty snowflakes as the growth becomes too heavy to be supported by the fragile dendritic trees.

Gradually, the ice fragmentation and the condensation cloud diminish in intensity, and as the simulated hydrometeor warms through 0°C, the accumulated ice starts to melt. The melting process is not instantaneous over the surface of the object, but starts from the top and advances slowly downward, taking as long as 5-10 minutes before melt water begins to drip from the bottom.

These visual observations suggest that the charge carriers in the separation process are the miniscule ice particles described above. For a qualitative confirmation of this, two 3" diameter circular electrodes are

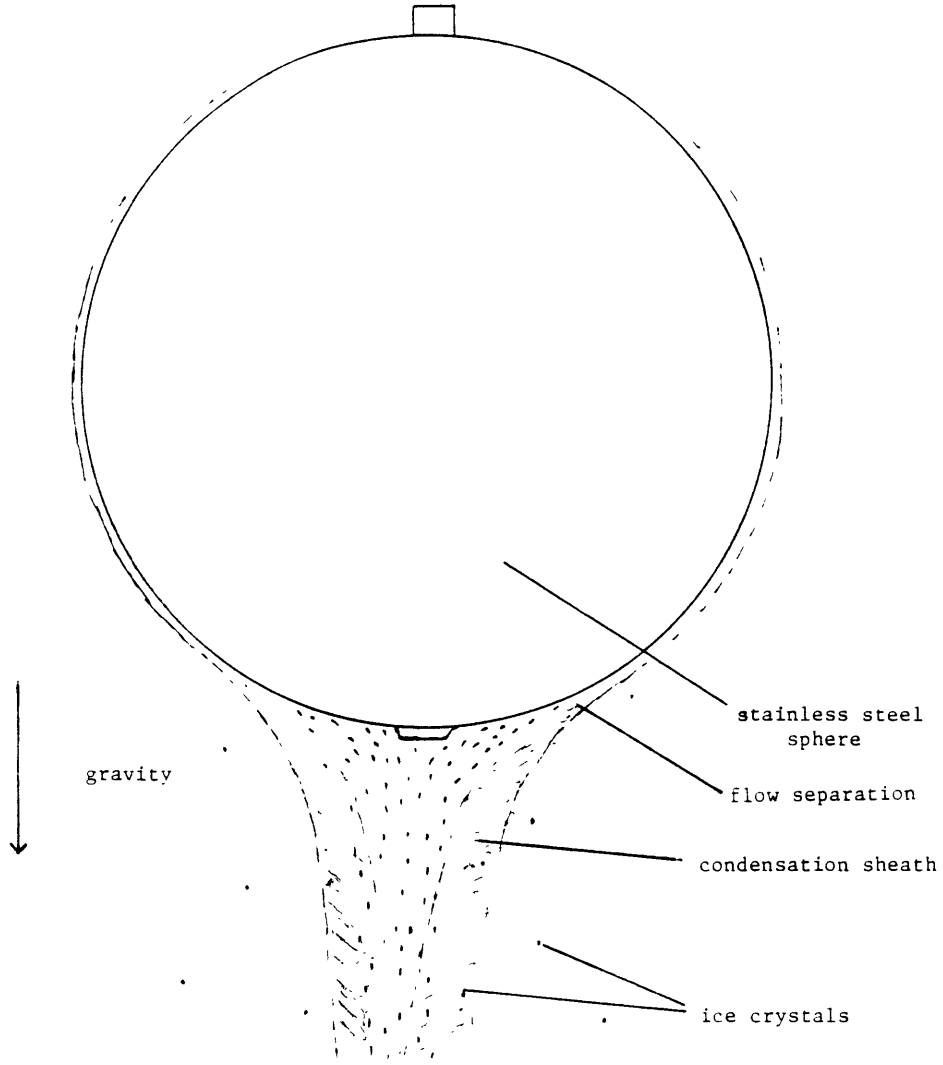

Figure 20 - Illustration of simulated hydrometeor in warm, moist environment of experiment chamber, with condensation sheath and ice crystals ejecting from the bottom of the sphere.

mounted 10 cm apart in the chamber such that the ice crystals and condensed cloud from a cold aluminum cup pass between them during frost growth. The electrodes are connected to a +1kV supply. When the voltage is applied, small ice fragments are deflected sideways and impact the positive electrode, indicating that they are negatively charged. It is difficult to discern if all fragments in the flow are deflected, but the condensation sheath appears unaffected by the applied field, as do the larger chunks of dendritic growth falling from the specimen.

Further visual evidence and measurements support the idea it is the small ice particles alone which are the charge carriers in these experiments. In viewing a frosty specimen in the growth chamber, the ice fragments can be seen falling into the pan under the weight of gravity. The supercooled cloud billows over the pan edge, though, and thus a considerable percentage of droplets do not ever come into contact with the pan-electrode. Hence, if the droplets were charged, the pan would not be registering the total current that was being separated from the hydrometeor. Figure 21 shows two separate runs done with STS at T_S=-17°C, T_C=41°C, RH_S=88%. Fig 21(a) is a standard trial with the pie pan for electrical measurement, while 21(b) is done with the sphere connected directly to the ammeter, with the pan removed. The polarity of 21(b) has been reversed, and with this change, the traces are indistinguishable. Hence we can conclude that the pan is indeed collecting all of the charge carriers, which are the ice particles, and that the supercooled drops do not have a measurable charge.

In viewing the frost growth during regular runs, though, it seems that

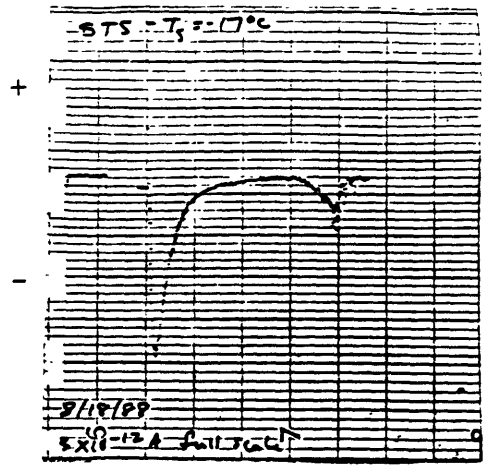

(a)

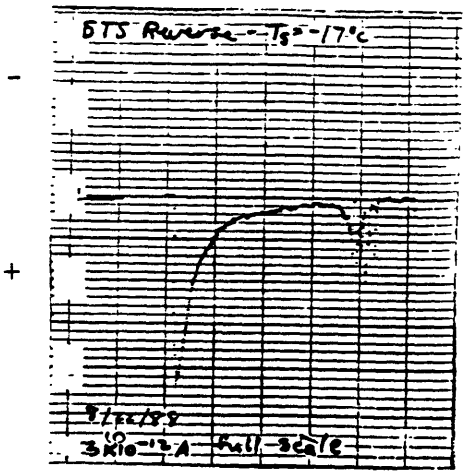

(b)

Figure 21 - Two runs with STS at Ts=-17°C, Tc=41°C, RHs=88%, full scale = 3 pA. In (a) the ammeter is connected to the pie pan, while in (b) the ammeter is connected directly to STS. Note the polarity is reversed in (b).

the pie pan current diminishes more rapidly in the initial growth peak than does the concentration of fragments ejected from the surface (i.e. When the current has already dropped off to near zero at a particular ammeter setting ten minutes or so into a run, there is still a substantial ice crystal 'snowstorm' beneath the simulated hydrometeor). Unfortunately, a quantitative measure of the relative intensity is not available.

This observation is evidence that the charge separation is dependent on the state of the surface from which the splinters are ejecting. More specifically, it hints that somehow the initial deposition process of frost on a substrate is electrically active while later growth on a frost substrate is inactive. A simple way to test this hypothesis is an experimental run with a metal simulated hydrometeor that has a layer of frost already deposited on the surface at the beginning of the trial.

The test is done first with STS at T_S=-20°C, T_C=28°C, RH_S=93%, because this combination has a strong signal to noise ratio and yields consistent and reproducible results (See Fig. 8). The I_{max} values for this set of conditions range from 1.2 to 1.5 pA (from the specimen). To prepare the sphere, the normal procedure for a standard current measurement run is followed. STS is frozen to -20°C and placed in the chamber environment at T_C=28°C, RH_S=93%, and the ammeter needle is monitored. Approximately 5 minutes into the trial, when the frost growth peak is essentially complete and the pie pan current has returned to nearly zero (on the 3 X 10^{-12} A full scale setting), the sphere is quickly pulled from the drum and set back into the freezer.

Several hours later, when STS has returned to equilibrium with the air in the freezer at -20°C but the frost growth has not yet appreciably sublimated (i.e. none of the bare metal is exposed), the current measurement is repeated with T_C=28°C, RH_S=93%. For this run the current peak associated with frost growth yields a maximum of -.12 pA to the pan, which is approximately one tenth of the maximum of the regular non-frosty trials. This result is illustrated in Fig. 22. Fig. 22(a). is a regular run, done in the standard fashion, while 22(b). is a trial using STS pre-frosted. Note that the current scales are different for the two traces.

This procedure is repeated with AL1 and AL2 at T_S=-26°C, T_C=28°C RH_S=93%, and the results are similar. In all cases the maximum current transferred in the frosty run is at least an order of magnitude less than the values obtained from the clean metal surface with the same initial conditions.

The procedure for pre-frosted runs described above brings to mind perhaps a better means of testing a smooth ice surface for charge separation. By coating STS with water from a spray bottle and allowing it to refreeze to a desired T_S, we would have an ice substrate whose temperature could be monitored in the manner of STS in regular runs. Four trials with this method at T_C=41°C, T_S =-20°C, RH_S=88%, yield I_{max} values evenly distributed between .23 pA and 1.8 pA from the 'rimed' sphere. With this amount of variance, we suspect problems in repeatability similar to those with the ice hemispheres. Specifically, an inability to control the growth (and hence electrical) state of the ice

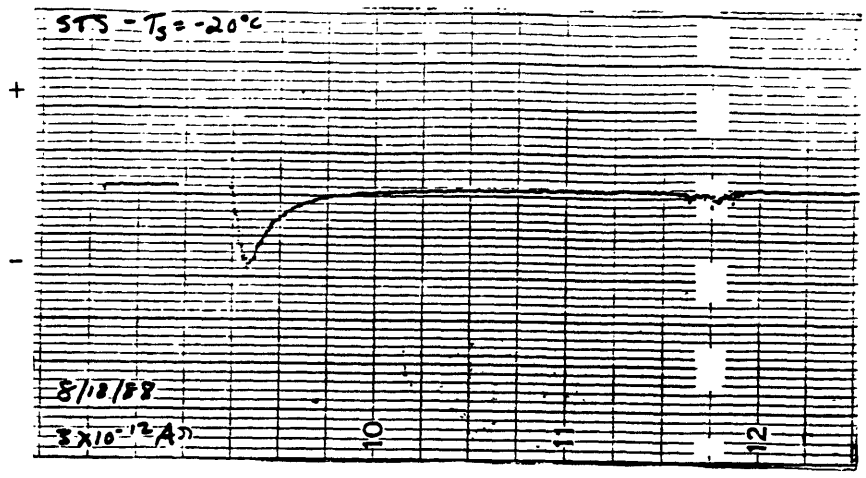

(a)

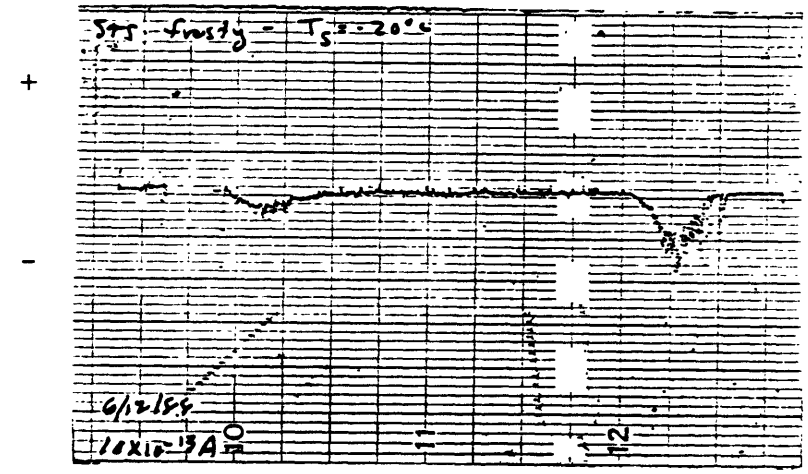

(b)

Figure 22 - Two current traces with STS at Ts=-20°C, Tc=41°C, RHs=88%. (a) is a regular trial, full scale = 3 pA, while (b) is a run with pre-frosted STS, full scale = 1 pA.

surface in the fluctuating temperature environment of a thermostated freezer. Hence, though this line of experimentation is not pursued further, the variance observed reinforces the notion that the presence or absence of a separation current during frost growth is strongly controlled by the degree to which H_2O molecules have been deposited on the substrate from the vapor.

We now shift our attention to the observation that, during regular runs, ice crystals are seen emanating only from a limited area on the bottom surface, and not the entire specimen. The ejection appears highly nonuniform in the active region, which we estimate to be about 50 cm^2 for the 6" objects. This is consistent with the fact that, though the aluminum cups have a substantially smaller surface area than the stainless steel sphere, the magnitudes of I_{max} are very similar for the different geometries at both T_C=28°C and T_C=41°C. A definitive test, however, is needed to show that splintering and charge transfer are not simply proportional to the total surface area of the simulated hydrometeor.

The experiment devised for this purpose involves a .875" thick circular solid aluminum slab which has a diameter of 8.875". The disk is threaded at the center of the circle and also at a point perpendicular to this on the outside rim to fit a steel screw handle from which the slab is supported. Thus, with the handle in the vertical, the slab can be mounted in two different orientations in the experiment chamber--with the flat face down or with the curved .875" thick rim facing down. The test, then, is to grow ice on this specimen in the two different orientations but with identical

temperature/water vapor boundary conditions and compare the current transfers. If the charge separation depends only on total surface area, the traces should be the same.

For this experiment, the pie pan electrode is abandoned. During a run, the handle supporting the aluminum slab is attached to a length of .5" diameter Teflon rod mounted at its other end to the stainless steel support rod in the drum. The handle/Teflon and Teflon/chamber rod connections are made with Fisher laboratory clamps. Thus the aluminum disk is electrically insulated from the chamber, and can be connected directly to the ammeter lead via alligator clips. With this arrangement we have a direct measurement of the current transferred from the specimen during frost growth.

In this experiment the slab starting temperature (T_S) is -24°C and the chamber environment is T_C=41°C, RH_S=90%. At the start of a run the slab is removed from the freezer and quickly mounted to the Teflon rod in the can. The alligator clip is connected and current is then recorded on the Rustrak. The results from trials at the two orientations (shown in Fig. 23) are substantially different. With the flat face down the maximum current reading is 6 pA, with a total charge transfer in the frost growth peak of 1340 pC. With the disk rim down, on the other hand, I_{max} (from the slab) =1.6 pA, Q=168 pC. Thus, we have about a factor of 4 difference in maximum current and almost an order of magnitude difference in total charge separated.

This is striking evidence that only parts of the surface area of a cold

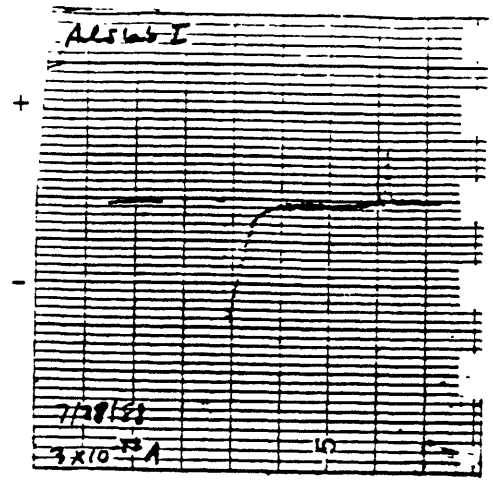

(a)

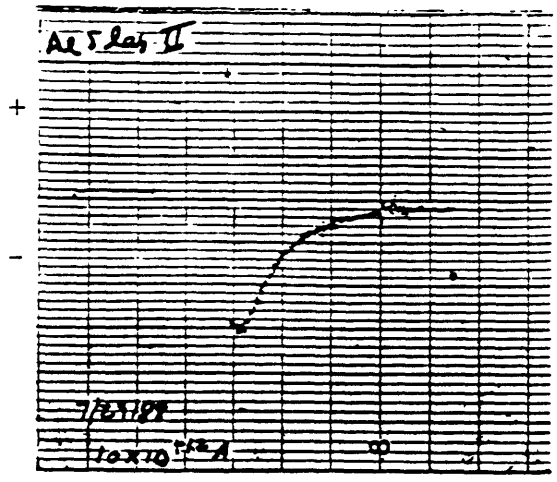

(b)

Figure 23 - (a) current trace from aluminum slab in vertical orientation, full scale = 3 pA, & (b) trace from aluminum slab in horizontal orientation, full scale = 10 pA.

object participate in electrified ice splintering. In observing the above runs through the chamber viewing hole, it seems that the ejection activity again is confined to downward facing regions. Indeed, the downward facing area of the disk in the first orientation is 62 in^2 , compared to approximately 14 in^2 for the edge down mount (i.e. the semicircular strip area of the slab). The ratio of these areas is close to the factor of four difference in I_{max} for the two cases. The surfaces of the Al cups and the stainless steel sphere are identical in area and shape from the equator down to the bottom pole. Hence the above result suggests that the maximum I_{max} values should be comparable for the cups and spheres (ignoring the differences in metal type). The agreement with the measurements discussed in the Data section is additional evidence that metal type is of secondary importance in this phenomena.

In working with the aluminum slab, we observe that the object appears to warmup uniformly during experiment runs (i.e. As the slab warms through the freezing point, the accrued frost melts on the entire specimen almost simultaneously). This feature allows for a quick and easy determination of the total ice growth on the slab during a run. Using a Mettler AE163 digital scale, several paper towels placed in a styrofoam cup are weighed before a run. The run is then conducted with the slab such that, as the frost begins to melt, the object is pulled from the experimental chamber and the melted ice is quickly collected with the paper towels. The towels and styrofoam cup are then reweighed and the difference in the pre- and post-weighings represents the total mass growth during the trial.

Performing this procedure three times each with the slab in the vertical and horiztontal orientations, we obtain an average mass growth for the smaller current, vertical mount of 9.5 grams (standard deviation = .5 g) and an average of 7.9 grams (standard deviation = .2 g) for the horizontal orientation. Qualitativlely, this result seems reasonable because the slab in the vertical should experience a greater degree of riming and, because a smaller area is apparently involved in ice crystal splintering, the ejected mass should be less. Thus, the total accrued mass is greater even though the charge transfer is significantly less. From this, it can be concluded that mass growth on a simulated hydrometeor cannot be used as a proxy variable for the total charge separated.

Before proceeding to an interpratation of the numbers in the Data section, we report the results of two attempts to modify the condensation sheath enveloping the growing specimen in the cloud chamber with the aim of gaining insight into the importance of riming in the charge separation. The first is a test of whether increasing the CCN concentration in the drum has any effect on the experimental results. The chamber is flooded with cigarette smoke through the viewing hole, and several pie pan current vs. time trials are done with the stainless steel sphere at T_S=-17°C, T_C=41°C, RH_S=88%. Two runs with these conditons yield current maxima to the pan of -2.8 and -2.7 pA with total charge transferred in the frost growth peaks of 300 pC and 290 pC respectively. A check of Figure 3 and Table 2 shows that these values are indistinguishable from the results with laboratory air in the chamber. Hence, the smoke makes no distinguishable difference with these run conditions.

The second test involves burning a small (2 cm^2) section of paper stained with silver iodide (AgI) in the can just prior to a run with T_S=-17°C, T_C=41°C, RH_S=88%. Again the result is indistinguishable from a 'regular' current trace. The negative results from these two attempts to modify the droplet population alone do not tell us a great deal about the relative importance of riming in our experiment. However, the tests do suggest that perhaps the riming rate is not a fundamental aspect of charge separation. It is possible, though, that supersaturations in the boundary layer are such that homogeneous nucleation dominates, with heterogeneous nucleation playing only a secondary role. In this case, smoke would have no impact on the degree of riming. We will commment on this possibility further in the next section.

The supplemental experiments described above yield a great deal of information about the charge separation phenomena in general. We have strong evidence that the charge carriers are miniscule ice particles emanating from a localized area on the bottom facing region of a simulated hydrometeor during growth in a warm, moist environment. The results also reveal that the charge separation during frost growth is strongly dependent on the degree to which H_2O molecules have been deposited on a frost free substrate, and that the type of substrate is probably of secondary importance.

Interpretation

With these results in mind, we shift our focus to an interpretation of the trends in the numbers presented in the Data section. Specifically, we now attempt to account for the variation across T_S seen in all of the sets of data at any one can temperature, T_C. Again, we deal primarily with the STS data because it shows the greatest reproducibility. Data in Fig. 4 (from T_C=41°C, RH_S=88%), with the peak in I_{max} values (T_{Smax}) around T_{bimax}=-14°C, is suggestive of the well-known curve of depositional mass growth rate vs. temperature of an ice crystal as developed by Mason (1953), which has a peak in the growth rate at -14.25°C at 1000 mb. However, Mason's analysis is valid for supersaturations very close to one in a growth environment with steady state temperature and vapor fields such that the ice crystal is slightly warmer than the ambient environment, with a balance achieved between the release of latent heat by deposition on the crystal and the diffusion of heat from the crystal to the environment.

These constraints are not applicable to the growth of ice on the simulated hydrometeor in our experiment chamber. In a simplified analysis for the stationary case (ignoring ventilation effects), we have the diffusion of vapor down a temperature gradient with deposition and the release of latent heat on a substrate which is a large heat sink and is essentially a perfect conductor. Since the temperature in the air above

the ice must be higher than the surface itself (because the surface is inducing the temperature perturbation in the ambient chamber environment), the conduction of heat must always be into the substrate.

If we assume that, as deposition is just beginning, the latent heat released from deposition of vapor to form frost is communicated directly to the substrate (i.e. The accumulation of frost is too thin for the thermal diffusivity of the ice to become a limiting factor), then the growth rate will be controlled by the diffusion of water vapor only. The mass growth rate from diffusion alone on a hydrometeor of radius R is given by (from Rogers, 1979):

$$dm/dt = 4\pi R^2 D \, (\partial\rho/\partial r)_{r=R} \qquad (1a)$$

where D = diffusivity of water vapor in air

For the steady state solution of the diffusion equation this becomes:

$$dm/dt = 4\pi R D \, [\rho_c - \rho_{si}(T)] \qquad (1b)$$

where ρ_c = ambient vapor concentration

$\rho_{si}(T)$ = ice surface vapor concentration

In the expression above, D varies slightly with temperature, and $\rho_{si}(T)$, which is just the saturation vapor density over ice at temperature T, is very

small ($\leq$ 1 gm/m^3 below -10°C) in comparison to ρ_c in our experiments. Thus, the mass growth is dominated by ρ_c, which is constant for any set of runs at one can temperature. This suggests that, perhaps for the first few minutes of a run (when most of the charge separation generally occurs), the accumulated mass should be more or less independent of T_s at constant T_c.

Before continuing with this line of thought, though, we must assess the importance of ventilation on the mass growth rate. The effect of ventilation is to contract the disturbance of the ambient vapor field to a small boundary layer around the sphere. This contraction steepens the local vapor gradient around the simulated hydrometeor and thus enhances the mass growth rate. In Mason's (1953) treatment, he obtained a simple analytical expression for this enhancement by assuming the diffusion boundary layer could be modelled as the vapor field at time = t around a spherical ice particle introduced initially into an undisturbed medium of density $\rho = \rho_c$ at t_o. The expression Mason obtained for the vapor gradient at the surface of a hydrometeor of radius R is given by:

$$(\partial\rho/\partial r)_{r=R} = (\rho_c - \rho_{si}(T))\ [\ 1/R + 1/(\pi Dt)^{1/2}] \qquad (2a)$$

Substituting into (1a) this becomes:

$$(dm/dt)_{ventilated} = (dm/dt)_{static}\ [\ 1 + (R^2/\pi Dt)^{1/2}] \qquad (2b)$$

where D is the diffusivity of water vapor, and t is the time the perturbed diffusion field has had to spread out from the particle. If we have a flow velocity, U, around a sphere of radius R, then a parcel of air in the flow will be in contact with the sphere for a time given by:

$$t = (2R/U) \tag{3}$$

before it is replaced with a fresh parcel. Thus, the mass growth will be increased by a ventilation factor, f_v, given by:

$$f_v = 1 + (UR/2\pi D)^{1/2} \tag{4}$$

but this is just (from Keller, 1980):

$$f_v = 1 + 1/(2\sqrt{\pi})\ S_c^{1/2} R_e^{1/2} \tag{5}$$

where $S_c = \nu/D$ (6)

ν = kinematic viscosity $\approx 1.5 \times 10^{-5}\ m^2 s^{-1}$

D = diffusivity $\approx 2.1 \times 10^{-5}\ m^2 s^{-1}$

and $R_e = (2UR/\nu)$ (7)

(S_c is the Schmidt number and R_e is the Reynold's number).

To get an estimate for the velocity (U) in a buoyancy induced flow around

a sphere of characteristic length L = 2R in a region of density disturbance $\Delta\rho = \rho_1 - \rho_2$, where ρ_1 = cold air densisty and ρ_2 =warm air density, we can equate the kinetic energy produced per unit volume, $\rho_1 U^2/2$, to the work input of the buoyancy force per unit volume acting over a distance L, $gL\Delta\rho$, to get (from Gebhart, 1987):

$$\rho_1 U^2/2 \approx gL\Delta\rho \quad \text{or} \quad U = O\left[(4Rg\Delta\rho/\rho_1)^{1/2}\right] = O\left[.8\ ms^{-1}\right] \tag{8}$$

Substituting this back into (7) yields:

$$R_e = 2RU/\nu \propto (8R^3 g\Delta\rho/\rho_1\nu^2)^{1/2} = G_r^{1/2} \tag{9}$$

where G_r is the Grashof number. Thus, if we assume that $G_r^{1/2}$ is a fair approximation for the Reynold's number, we can compute the ventilation coefficient as:

$$f_v = 1 + 1/(2\sqrt{\pi})\, S_c^{1/2} G_r^{1/4} \tag{10}$$

or

$$f_v = 1 + .24\, G_r^{1/4} \tag{11}$$

In Table 4 we have listed values of G_r and f_v for T_s=-50°C, -20°C, and 0°C

Table 4 - Grashof number (G_r) and mean ventilation coefficient (f_V) for different experimental conditions

T_S, T_C (°C)	G_r (X 10^7)	f_V
-50, 28	3.4	19
-20, 28	2.5	18
0, 28	1.3	15
-50, 41	3.9	20
-20, 41	3.2	19
0, 41	2.1	17
-50, 52	4.2	20
-20, 52	3.5	19
0, 52	2.4	18

density of air (kg/m^3)

$\rho_{-50} = 1.51$

$\rho_{-20} = 1.40$

$\rho_0 = 1.29$

$\rho_{28} = 1.18$

$\rho_{41} = 1.12$

$\rho_{52} = 1.09$

at T_C=28°C, 41°C, and 52°C to illustrate the range of numbers encountered in these experiments (with L=.15m, g=10 ms^{-1}, $\nu \approx 1.5 \times 10^{-5}$ m^2s^{-1} and ρ listed in the table, from Gebhart, 1987). We see that within a particular chamber temperature, as is expected, the ventilation coefficient decreases with increasing T_S. However, the changes in f_V are fairly modest considering the large range in ΔT at any one T_C from T_S=-50° C to T_S=0°C. This is largely because of the cubic dependence of the Grashof number on the length scale, which is of course constant.

Now, with the effects of ventilation included, we have a mass growth equation given by:

$$dm/dt = f_V(T)\, 4\pi DR\, [\rho_C - \rho_{Si}(T)] \qquad (12)$$

This relation yields a mass growth rate across T_S (for one T_C) that is relatively constant, with a slight increase with decreasing temperature. Eqn.(12), however, does not account for riming, which should increase dm/dt, or the fact that condensation in the boundary layer will probably diminish the actual vapor gradient at the ice surface, which would cause a decrease in the mass growth rate.

Probably more importantly, though, at least in terms of variation across one set of T_S runs, is that the simple treatment above does not include surface kinetic effects (i.e. the effects of variation in crystal habit), which have been shown to be controlled strongly by ice temperature, over a range of temperature considered in our experiments. This evidence is illustrated in

Figure 24, which is a plot of data obtained by Hallett (1965) in which he grew individual ice crystals at various temperatures at water saturation in a diffusion chamber. The results, depicting 'real' single ice crystal growth rates, show order of magnitude enhancements near -5°C and -15°C that must be attributed to surface kinetics. Note that these numbers are for single ice crystals in an environment in which there is no other competition for water vapor. We would expect the enhancement per unit mass to be considerably less for our case in which a field of crystals are competing for the available vapor above a substrate. Thus, with this effect in mind, we might expect in reality a dm/dt vs. T_S which is fairly flat with T_S, with perhaps an increase in growth rate near -5°C and -15° C.

We must also remember that Eqn. (12) was developed assuming the latent heat of deposition is instantaneously dissipated into the substrate. Obviously, as growth proceeds and the frost deposit becomes thicker, this assumption becomes less and less valid. Because of the finite thermal conductivity of the ice, continued release of latent heat at the surface will result in a temperature gradient through the frost growth. Eventually, a quasi-steady state should be reached in which in which the release of latent heat by deposition coupled with the diffusion of heat from the $(T_C - T_{Si})$ gradient is balanced by the diffusion of heat through the interior of the ice into the substrate. This becomes a complicated problem which we will not address here. It is sufficient to say that this will result in a gradual departure from Eqn. (12) with a decrease in the mass growth rate that will be augmented as the sphere warms up.

We have devised a simple means to test how well Eqn. (12) can be used to

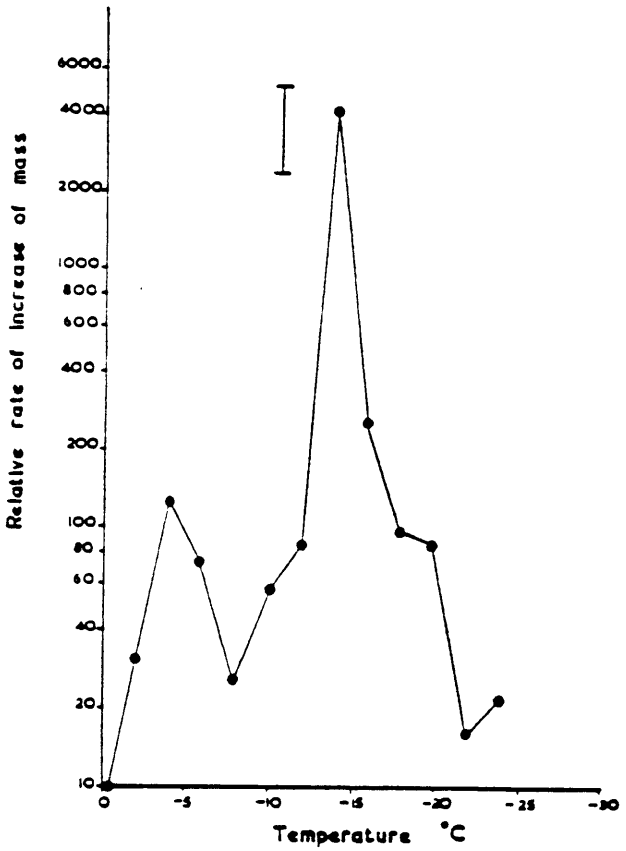

Figure 24 - Relative rate of mass increase of crystals growing at water saturation in a static environment. From Hallett (1965)

describe the mass growth on STS for the first few minutes of a run. The mass is determined by the following simple procedure similar to that described for the aluminum slab above: a plastic bag, several paper towels and a styrofoam cup are weighed beforehand on the Mettler AE163 digital scale. STS at the desired T_S is then placed into the chamber at the desired T_C and relative humidity for 120 seconds, at which time the cover is removed and the plastic bag is placed carefully over the sphere, with a minimum of air in the bag. The bag is secured with a tie around the mount screw at the top of STS to close the system. After 20-30 minutes, when the accumulated frost on the sphere (and inside the bag) has melted, the condensation on the outside of the plastic is wiped off and the bag is removed. The remaining moisture on the sphere is quickly collected with the paper towels, which are then reweighed in the styrofoam cup on the scale. The difference between pre- and post-weights represents the ice mass accrued in the 2 minutes of frost growth. This is a crude method, to be sure, but if the collection is done quickly (to minimize evaporation) and carefully it should be valid.

It is difficult to estimate the error in this measuring techique without actually repeating the procedure many times, but it is likely that, if anything, the weighing will yield a value greater than the true mass growth. As a one-time assessment of this error, the mass determination is conducted such that the ice free STS is secured in the plastic bag before the specimen is removed from the freezer. Thus, if the method is accurate, the difference in the two weighings should yield a value close to 0.0 grams of ice growth. In this trial, the post cup weight is .11 grams heavier than the initial number. With this result we are confident that our measurements are likely within .15

grams of the true value.

Two 2-minute mass measurements at T_c=41°C, RH_s=88% (ρ_c= 45 gm^{-3}), are done--one at T_s =-50°C (ρ_{si}= .07 gm^{-3}) and the other at T_s=-17°C (ρ_{si}= 1.2 gm^{-3})-- and yield values of 2.0 g and 2.2 g H_2O respectively. With D=2.1 X 10^{-5} m^2s^{-1}, R = .08 m, and f_v values from Table 4, we calculate mass growths from Eqn. (12) of 2.3 g and 2.2 g H_2O respectively. Thus, these two measurements suggest that Eqn. (12), perhaps modified for an enhanced response at -5°C and -15 °C for surface kinetic effects, is not a bad approximation for the total mass growth on the sphere for the first few minutes of a run.

With these two mass measurements nearly equal at two run conditions which yielded a factor of five difference in I_{max} (from Fig. 4), it is difficult to argue that charge separation is proportional to the frost growth rate on the simulated hydrometeor. However, we must remember the earlier evidence that ice particle ejection appears to be confined to a limited area on the sphere, and not the entire surface, and that this 'active' area is in a region where the buoyancy induced flow is separated from the sphere . Thus, ventilation effects and probably also the vapor gradient for diffusion are substantially smaller than over other parts of the object. Therefore, changes in the mass growth rate on the bottom facing areas of interest might well follow the variation in charge separation vs. T_s, but we might not be able to see this in the changes in the 2 minute mass growths for the entire sphere across T_s at one T_c.

We can also use the 2-minute mass growth measurement to compare the frost accumulations at the three different can temperature/humidity environments used in the experiment as a further test of the validity of Eqn.(12). Table 5 is a summary of the STS data, listing can temperature (T_C), water vapor content (ρ_C), the maximum I_{max} reading in the set (I_{max}'), and its corresopnding T_{bimax}, where it is available, for the three environments, labelled I, II, and III. Again, Eqn. (12) suggests that the 2-minute mass growth at any one T_S value should increase almost linearly with the increase in ρ_C from I to II to III. Specifically, for three runs at T_S =-17°C --one at each of the three environments listed in Table 5--the predicted 2 minute frost growths (with f_V values from Table 4) are 1.1 g, 2.2 g, and 3.2 g H_2O respectively for I,II, and III. A measurement at T_S=-17°C in environment I yields 1.2 g in 120 seconds, and in a run with the same T_S and environment III, we get a 2 minute mass of 3.2 g. Thus, with the 2.2 g H_2O value obtained above at T_S =-17°C , T_C =41°C, RH_S==88% (environment II), it appears, again, that Eqn. (12) is a good approximation for the total mass growth on STS for the first 2 minutes of a trial. These mass growth measurements, along with the predicted values from Eqn. (12), are also shown in Table 5.

If we assume that charge transfer is proportional to the growth rate of ice on the bottom of the sphere, then the growth behavior outlined above, with

Table 5 - STS summary

#	T_c (°C)	ρ_c (gm/m^3)	I_{max}' (pA)	T_{bimax} (°C)	2 minute mass values Eqn.(12)(g)	measured(g)
I	28	26	1.55	-18	1.1	1.2
II	41	45	2.8	-13	2.2	2.2
III	67	67	12.0	*	3.2	3.2

initial deposition moderated by the diffusional growth rate and temperature dependent surface kinetics alone, and then a gradual buildup of a temperature gradient through the ice due to continued latent heat release at the surface and a resulting diminishment of the growth rate, can be used to qualitatively account for many of the principal features and trends in the current traces. When the simulated hydrometeor is placed into the chamber at the beginning of a run, the full diffusional growth rate will not be achieved until perhaps a monolayer of frost (providing a ρ_{si}) has been put down on the bare metal substrate. Thus the growth rate and hence current peak does not occcur instantaneously, but there is some finite time to maximum charging (t_{imax}). The speed with which this frost layer can be deposited will depend partly on surface kinetics, which exhibit a maximum effect around -15°C, and will also depend on ρ_c. Hence, t_{imax} has a minimum close to -15°C for any one T_c (See Figs. 4A & 8A), but generally decreases as we move from environment I to II to III. Similarly, the maximum growth rate at any one can environment will

occur where the effects of surface kinetics are strongest (i.e. near -15°C), and this maximum will increase with the vapor gradient (increasing ρ_c). This is exactly the behavior of the of the I_{max} data.

As the growth proceeds and a temperature gradient develops in the accreted frost, the surface becomes progressively warmer than the metal substrate and the growth rate is subsequently reduced by the shrinking vapor gradient (because ρ_{si} increases). Thus the current magnitude falls off relatively quickly even though $\overline{T}_{bimax}$ rises slowly. However, at the lowest starting temperatures (T_s) for which the thick insulating frost layers are shed from the bottom of the object, as discussed in the previous section (p.59), the colder areas close to the metal surface are continually re-exposed and thus electrically active growth is re-'activated', causing an extended or double peak in the current trace.

Though this qualitative explanation seems to work well for many of the observed features in this experiment, it cannot be used to explain the results with the pre-frosted simulated hydrometeors. Recall that current magnitudes in pre-frosted runs are an order of magnitude less than in regular trials with bare metal surfaces. Since there is already a frost surface on the substrate (and hence a ρ_{si}) in the pre-frosted cases, from the above qualitative explanation one might expect the current maximum to occur almost instantaneously in the trace. A look back to Figure 17 reveals that this is clearly not the case.

There is also a problem with the above explanation in that, as Table 5 reminds us again, the total frost growth clearly does not follow the increase

in I_{max}' from T_c= 28°C to 41°C to 52°C, which jumps by a factor of nearly 8 from environment I to III. As a further reminder of the dramatic increase in I_{max} across the three chamber environments, we present average I_{max} vs. T_s for the three sets of STS runs together in Figure 25. This plot is just a summary of the data in Figs. 4, 8, & 9. The T_s=-19°C, -20°C, & -21°C numbers at T_c=52°C are averaged for the T_s= -20°C, T_c=52°C point. Note also that the T_s=-14°C, -12°C, & -9°C numbers at T_c=52°C are 'averages' of a single data point.

To gain additional insight into what is controlling the magnitude of the charge transfer in this experiment, we perform a set of runs using STS at T_s=-17°C, T_c=41°C, with varying initial relative humidities, and thus we vary ρ_c while keeping T_c constant. Plotted in Fig. 26 are I_{max} data from these trials versus relative humidity at the time of I_{max} (RH_{imax}), which is a more accurate representation of the chamber water vapor content during growth of frost than the initial relative humidity, RH_s. The numbers suggest that I_{max} is constant above $RH_{imax} \approx 45\%$ all the way up to the experiment limit of RH_{imax}= 84%. Thus, over approximately a factor of 2 in water vapor content the results are indistinguishable, and hence, independent of relative humidity in the chamber. Below RH_{imax}=45%, it seems some threshold is crossed and the maximum current falls linearly to zero by RH_{imax}=18%.

Figure 25 - Summary of STS data from the three can environments

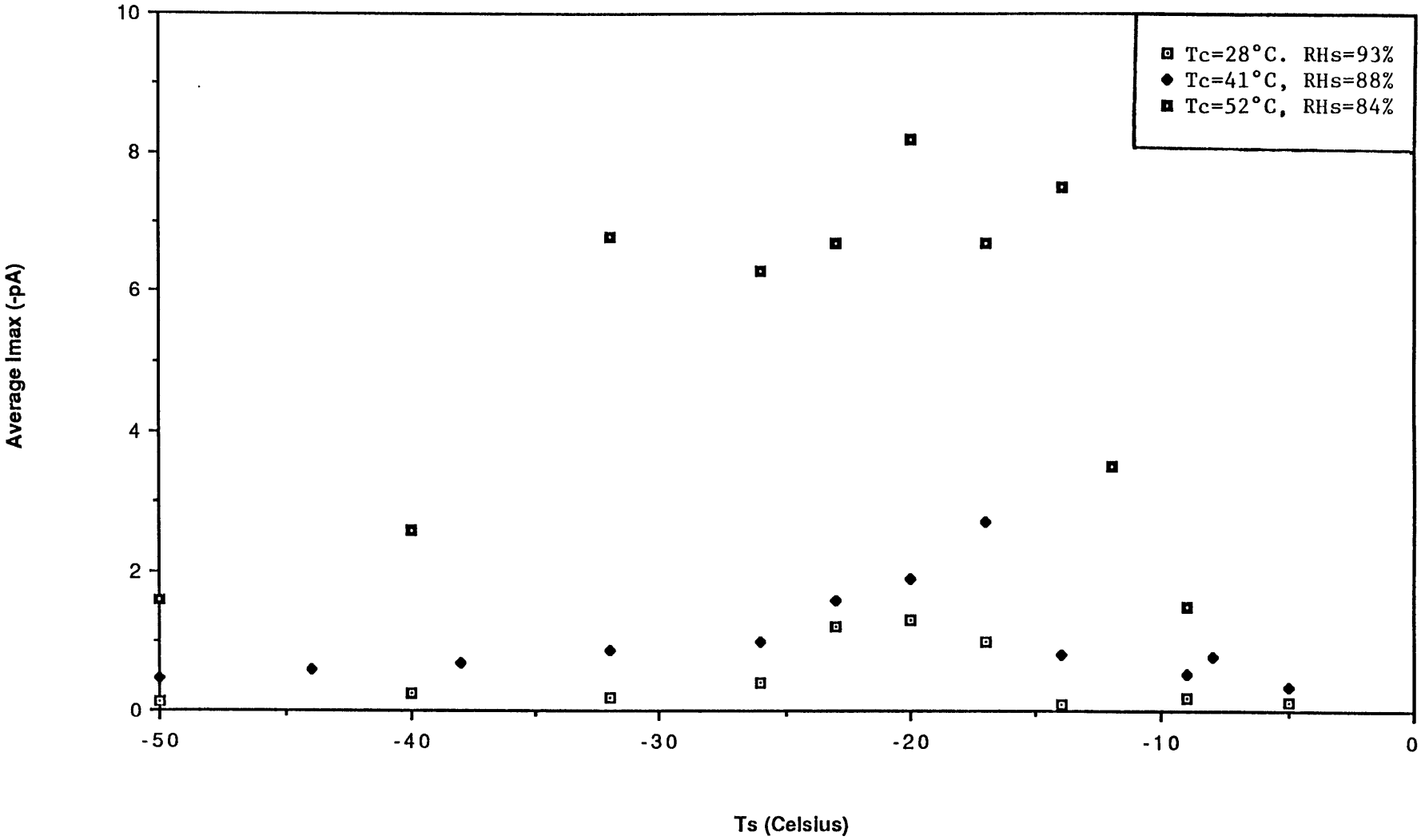

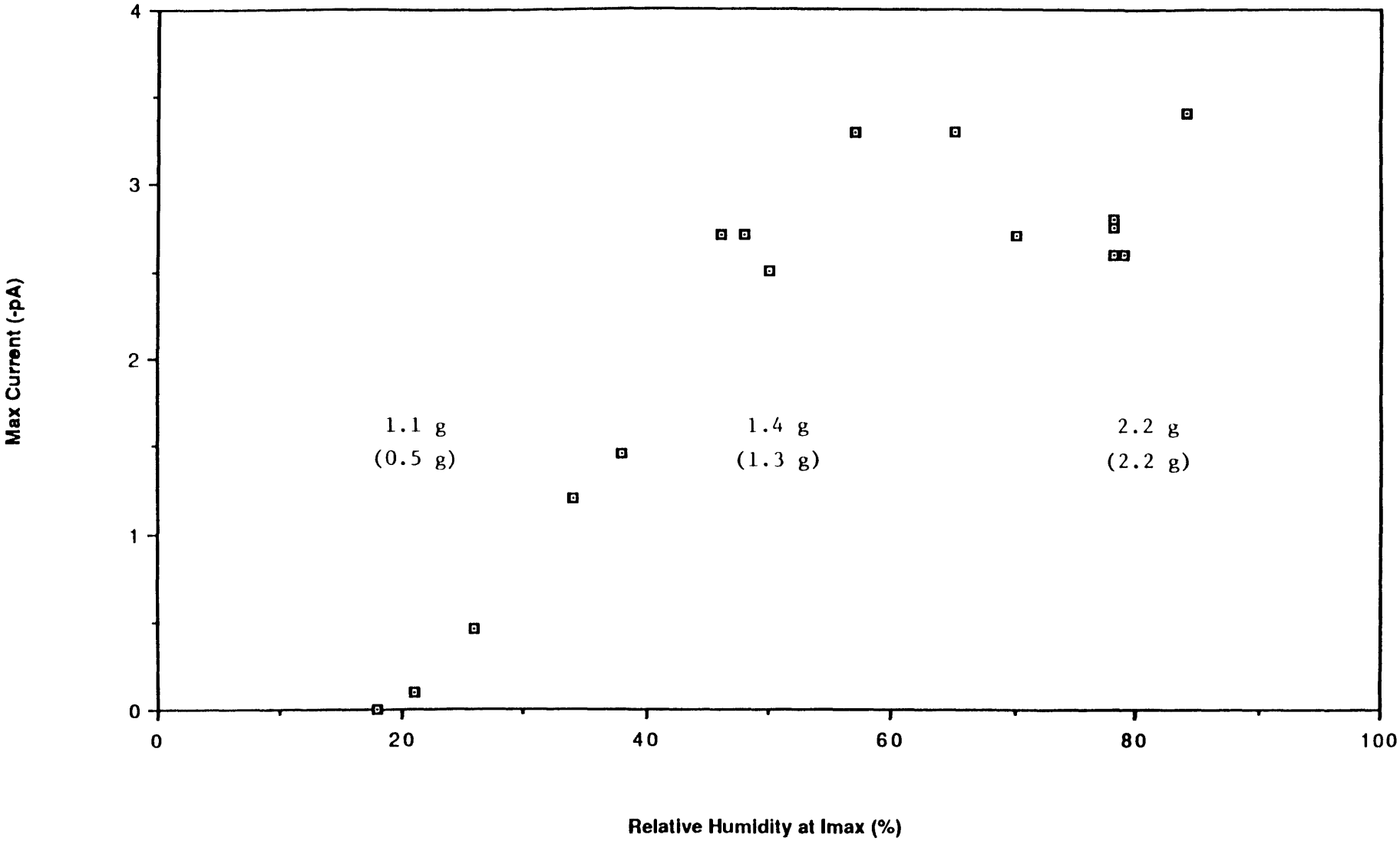

Figure 26 - Max current vs. RH in chamber with STS, Tc=41°C, Ts=-17°C. Also shown are three 2 minute mass growth measurements at RH=20%, 50%, & 80%, along with the predicted value from Eqn. (12) in parentheses.

The RH_{imax}=46%, T_c=41°C point, with an I_{max} magnitude of 2.75 pA, has a water vapor content of 26 g/m^3 in the chamber. Note that this is the same environmental vapor density, ρ_c, as in the trials with Tc=28°C and RHs=93% (see Table 5), which yielded an I_{max} for the three T_s=-17°C runs with STS of 1.0 pA (See Table 2), or nearly a factor of 3 smaller than the above.

Observations of the above runs show that below 45% RH_{imax}, a diminishment of the thick condensation around the specimen becomes noticeable. This seems to coincide with the drop-off in I_{max} with decreasing relative humidity such that, by RH_{imax}=18%, it is difficult to discern any condensation in the flow shedding from the specimen. It is interesting to note, however, that in this environment devoid of visible condensation in which the current signal has dropped into the noise, ice crystals reflecting in the chamber light can still be seen emanating from the bottom of the sphere. These observations suggest that, somehow, the presence of the condensation sheath beneath the electrically active, bottom facing region of STS might represent a limit to the vapor gradient (for a particular temperature gradient) that can be achieved at the surface in the areas where the buoyancy induced flow has separated from the object. Thus, as we move to environments with increasing water vapor above the threshold value, perhaps the vapor gradient, and hence the growth rate, is not increased but the excess vapor is 'bled' away as condensation. Of course this is mere speculation, as solutions for the temperature gradients in buoyancy induced flows do not extend to regions of flow separation, and thus the behavior in these areas of interest is not well

understood.

Also shown in Fig. 26 are three 2-minute mass growth measurements taken at RH_{imax}= 20%, 50%, and 80%, and with them, in parentheses, predicted values from eqn. (12) (The RH_{imax} = 80% number is from the T_s=-17°C, T_c=41°C, RH_s=88% measurement presented twice above). Generally, the measurements again agree fairly well with the calculations. However, it is peculiar that the RH_{imax} = 20% weighing exhibits a relatively large positive departure from the predicted value.

The observation that condensation is no longer visible in the boundary layer below RH_{imax} = 20% for T=41°C, T_s=-17°C is cause for a slight digression in our analysis. We take a moment to examine whether predictions from Mason's (1953) treatment are consistent with the above. The solutions for the vapor field, on which the analysis of the ventilation coefficient was based, can also be used for the temperature field such that we can determine the expected profiles of temperature and vapor pressure in the boundary layer. The temperature field yields the saturation vapor pressure as a function of r, and thus we can compare this with the vapor field to determine the supersaturation in the boundary layer.

We have computed the vapor concentration (in g/m^3) and temperature for six points in the boundary layer for T=41°C, T_s=-17°C, RH_{imax}=80% and 20%, and they are plotted together in Figure 27. (The details of the calculations are presented in Appendix D). Note the rapid rise in temperature with increasing r. The temperature numbers are converted to saturation vapor pressures and plotted with the vapor concentrations (converted to mb) in

Figure 28. Thus, the comparison of either trace with p_{sat} is a direct measure of the supersaturation state through the boundary layer. We see that $p_{20\%}$ is is undersaturated almost everywhere, but perhaps reaches saturation (with respect to water) between the ice surface and r' =1mm. This is consistent with the observation of no condensation in the boundary layer flow for this environmental condition. for the $p_{80\%}$ curve, on the other hand, supersaturations as high as 4-5 are achieved in the boundary layer. Supersaturations exceeding 6 are necessary for homogeneous nucleation to be significant (Pruppacher & Klett, 1980). With this result we are skeptical that homogeneous nucleation is occurring in the boundary layer flow.

Returning to the problem of the analysis of the charge separation, we see that though the approximation developed for the mass growth rate on the entire sphere for the first few minutes of a run seems to work well, and there is some evidence that the charge separation is a function of the mass growth rate on the bottom of the sphere, the variance in the data has still not been adequately explained. The surface state of the substrate (i.e. the degree to which H_2O molecules have been deposited) must be an important factor, though, as evidenced by the pre-frosted simulated hydrometeor results and the difficulties with water ice as a substrate for frost growth.

Another issue that must be considered further for understanding of the problem is the role of riming in the mass growth and charge separation phenomena. To what extent riming contributes to the mass growth of the simulated hydrometeor during a run is unclear. Though the condensation sheath is generally thick through a run, qualitative tests in which a laser

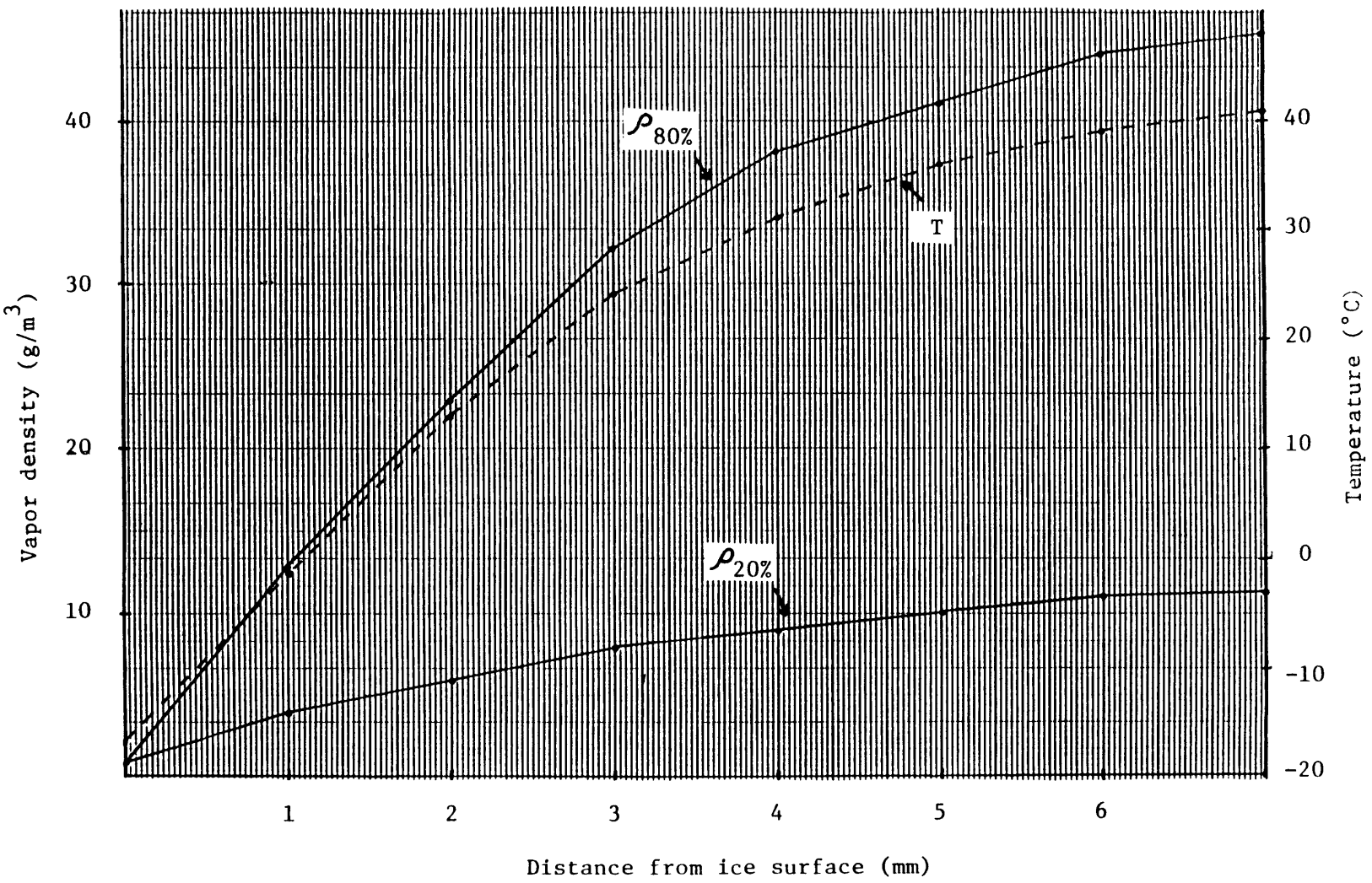

Figure 27 - Calculated boundary layer vapor density and temperature profiles for two runs at Tc=41°C, Ts=-17°C. Solid lines are vapor density, with the upper trace for RH=80%, and the lower trace for RH=20%. Dashed line is temperature.

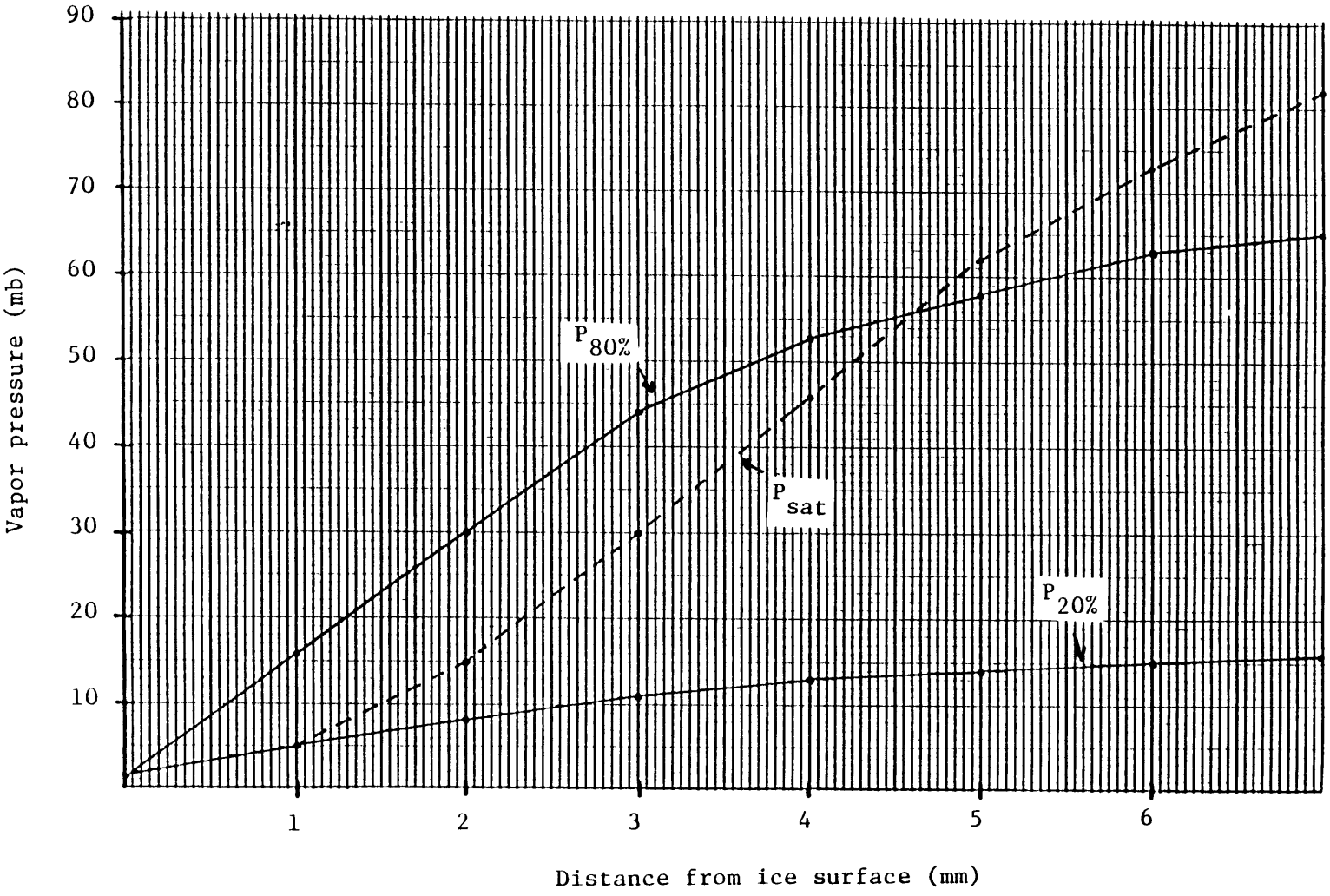

Figure 28 - Calculated boundary layer vapor pressure profiles for two runs at Tc=41°C, Ts=-17°C. Dashed line is saturation vapor pressure as determined from T profile in Fig. 26. Upper solid line is for RH=80%, and lower solid line is for RH=20%.

light is passed through the boundary layer of the condensation flow around a cold object in a warm and humid environment show a thin layer adjacent to the frost surface that is devoid of cloud.

However, if riming is a significant contributor to the frost growth, the possibility exists that it is also an important regulator of electrified crystal ejection. The fact that the principle ejection activity appears to be confined to bottom facing regions, which should experience a minimum amount of riming, might suggest that riming is suppressing charge separation on other areas of a simulated hydrometeor. Qualitatively, it also makes sense that accreting droplets on a dendritic tip would act to extinguish the rapid dendritic growth and, presumably, suppress the ejection and charge separation. As we move from environment I to II to III, with the increase in chamber vapor content, we expect the rate of riming on the specimen to increase, but we also expect an increase in the depostion rate. It is unclear which effect would predominate in the variation of I_{max} with T_C.

Unfortunately, with the bulk measurements and observations that have been detailed to this point, the uncertainties discussed above cannot be resolved. To do so we need information about the ejected ice fragments and the frost surface at the microphysical level, such as the charge per crystal, crystal habit, and crystal concentration at any particular hydrometeor starting temperature (T_S) and drum environment. Many and varied attempts to replicate ejected ice fragments and view them under an optical microscope were tried in an effort to make progress on these questions. The principal method employed for this task involves coating a glass slide with a 1% solution of Formvar in ethylene dichloride, allowing it to dry, cooling it in the

freezer to below 0°C, and then removing it and collecting a sample of ice crystals and droplets from the flow beneath a frost growing specimen either before or after the slide has been placed for 10 seconds in a can containing ethylene dichloride vapor. The slide is then returned to the freezer. The idea behind this technique is that when the cold slide is placed in the can, a small amount of ethylene dichloride vapor will condense on the formvar coated surface of the glass and dissolve a thin layer of the plastic in which the ice crystals are or can be caught in. The plastic is left with an imprint of the tiny fragments as the ethylene dichloride quickly evaporates, and when the H_20 molecules of the crystals have had time to sublimate from the slide in the freezer, the replicas in the plastic can be viewed under a microscope.

Theoretically, then, it would seem that using this technique, we could examine the habit and size of the ejected crystals versus T_S and also, with some type of temporal sampling, perhaps make some guesses about relative concentrations during a run, as in Jayaratne, et al. (1983). Unfortunately, the practical difficulties imposed by the experiment setup proved to be too great and these attempts were unsuccessful.

The main problem arises from the fact that the surface temperature of the formvar coated glass slide must remain below 0°C throughout the replication process or the tiny ice fragments will melt before setting. But a slide removed from below freezing temperatures to the warm and humid environment of the growth chamber instantaneously accrues a contaminating layer of condensation which alters, and hence ruins, the replication. To get an accurate representation it would be necessary to sample the ice crystal flow without subjecting the slide to warmer air. We could devise no simple and

effective means of doing this and so the formvar method was abandoned.

Thus, the only microphysical information we have come from Cheng's (1973) work in which he used an NCAR ice nucleus counter to measure the concentrations of crystal ejected from a growing 2mm diameter frosty ice pellet at different temperatures. He reported high concentrations at -5°C and -15°C (recall in this context Hallett's results, Figure 24) with needles and columns observed at the higher temperature and dendrites at -15 °C. Unfortunately, specific numbers at different temperatures are not available. Though these observations are not inconsistent with the hypothesis that the charge separation is proportional to the ice fragment ejection rate, clearly we do not have enough information to make a definitive statement.

On the basis of studies made of photomicrographs of frost growing in a warm moist environment, Scheafer & Cheng (1971) and Cheng (1973) suggested that the cause of this fragmentation is the sublimation of slender columnar attachments binding the crystals together as more massive structures growing on the frost surface compete for vapor. The strong dependence of charge separation (and presumably, ejection activity) on orientation in space, as demonstrated by the aluminum slab experiments, combined with visual evidence that crystal ejection appears to be confined to the bottom facing regions of frost growing specimens is perplexing and suggests that somehow gravity is involved, perhaps only in the sense that it determines the flow field around the sphere.

If the current is in fact proportional to the number of fragments ejected during frost growth, there is still no adequate explanation of why the particle separation is accompanied by a separation of charge which is so robustly one

sided (positive to the specimen, negative on the fragments). Again, qualitatively, an argument could be made that the thermoelectric effect is responsible. On a hydrometeor growing by vapor deposition, latent heat considerations dictate a surface warmer than the interior, with a resulting excess of negative charge residing there, in the manner of Latham and Mason (1961). Thus, sublimation combined with electrostatic repulsion would cause negatively charged crystals to be ejected from the surface. However, if this is the controlling mechanism in our study, how can it account for the relative absence of charge separation in the pre-frosted specimen trials? Even qualitatively, the thermoelectric explanation does not seem to hold up.

Before completing the Interpretation section, we once again shift our attention to the consideration of a robust feature that has been neglected to this point--the melting signature visible in all of the current traces shown in this paper. Like the peak associated with frost growth, the melting 'spikes' always transfer negative charge to the pan-electrode. Initially, the discontinuous nature of the signature suggested that it was the result of a Workman Reynolds effect, with drops of melted ice from the surface of the specimen causing the charge separation. In viewing runs through the observation window, though, it was noticed that the current signature is generally complete before the first drop of meltwater falls to the pan. In other words, drops of meltwater do not carry enough charge to register on the ammeter ($S/N \leq 1$). Careful observation reveals that current spikes are associated with enhanced ice crystal ejection from areas on the surface where advancing meltwater suddenly surges into a region of frost. The magnitude of a spike seems to be proportional to how much frosty area is

converted to water/water-ice in such a surge, and thus the trace is highly irregular from run to run. When the surface of the specimen has been cleared of frost , the signature is complete, and meltwater begins to drop into the pan. We have no plausible explanation for this phenomena, as it does not fall into a Dinger-Gunn or Workman Reynolds category.

Summary

These experiments have shown that the ice fragments ejected from a frost surface growing on a metal simulated hydrometeor in a warm moist environment are systematically negatively charged, independent of metal type. The maximum current transfer in a run increases with increasing specimen starting temperature (T_S) above -50°C to some maximum temperature (T_{Smax}), and also increases dramatically as the environment temperature and water vapor content are increased. The time to peak current also appears to be tied to specimen starting temperature. These trends with temperature in times to current peak and in the I_{max} numbers, particularly the T_{bimax} values near -15 °C for the stainless steel sphere, suggest that the charge transfer is somehow related to ice crystal growth rate, as demonstrated by Hallett's (1965) data which show a strong dependence on temperature, with a peak at -15 °C for ice crystals growing at water

saturation in a cloud chamber.

With the approximation that the ice growth rate in the first few minutes of a run is moderated only by the diffusion of water vapor across the buoyancy induced boundary layer around the sphere, with released latent heat of deposition comunicated directly to the metal substrate, calculations of the expected growth to the sphere for the first two minutes of a run for various environmental conditions prove to be a good estimate of the actual accumulation in that time as determined by weighing the melted frost. Unfortunately the mass growth rate developed from this approximation (which neglects surface kinetic effects and riming), does not yield a variation with temperature and water vapor content that is proportional to changes in I_{max} and its dependence on T_c and ρ_c.

However, observations of runs through the viewing hole in the experimental chamber suggest that the ejection of fragments occurs from only a limited area on the bottom pole of a specimen. This observation is reinforced by experiments with a circular aluminum disk, which reveal that the crystal ejection and current transferred from a growing simulated hydrometeor in a warm, moist environment is strongly dependent on the downward facing area of the specimen. Thus, it is not the total mass growth rate but only the mass growth rate for 'active' ejection regions that we are interested in. And it is these areas at the bottom of the sphere, where the condensation flow has separated from the surface, that the mass growth approximation is most likely to fail. Hence, though we cannot provide firm evidence that the ejection rate and current transfer is controlled by the depositional mass growth rate to a specific region on a specimen, our results

are not necessarily inconsistent with this hypothesis.

The simple approximation of the growth behavior of frost on the simulated hydrometeor in the experimental chamber does seem consistent with many of the observed features of current traces in the data, such as the finite time to maximum current at the beginning of a run and the presence of a double peak at the lowest T_S trials. However, current measurements with prefrosted simulated hydrometeors yield current values an order of magnitude less than trials with a pure metal surface. This result is evidence that the electrically active ejection is associated only with the deposition of the first layers of H_2O molecules on the frost free substrate. Also, though negative charge transfer is observed from water ice hemispheres and STS sprayed with water and then frozen, the results are not consistent and repeatable enough for analysis, probably because of our inability to control deposition and sublimation of molecules from the ice surface in the thermostat controlled freezer. This is further evidence that the presence or absence of charge separation is strongly dependent on the surface state of the substrate.

With limited microphysical information, it is difficult to explore possible mechanisms responsible for this phenomena. The aluminum slab measurements and observations suggest that gravity or orientation in the flow is important in the separation process in these experiments. The thermoelectic mechanism, as proposed by Latham & Mason (1961), is unlikely here considering the results with pre-frosted specimens and also in view of the fact that currents do not increase with increasing $\Delta T=T_C-T_S$ for a set of

runs at a particular chamber temperature (constant T_C).

Conclusion

The ultimate goal in studying this phenomena is to be able to relate the results to the atmosphere in an attempt to assess the possible importance of charge separation associated with frost growth in the electrification of thunderclouds. Trials at different chamber temperatures have shown that the maximum current transfer is not linear with $\Delta T=T_C-T_S$ for constant T_S, so it would be difficult to meaningfully extrapolate the results to realistic temperature gradients, which, again, are probably less than .5°C between a falling graupel particle and its environment. The trends in our data, however, suggest that there is a dramatic decrease in I_{max} with decreasing ΔT, and temperature and vapor gradients for hydrometeors in the atmosphere are 2-3 orders of magnitude smaller than in our experiments. Similarly, the dependence of total charge transfer on size is clearly not a function of the total surface area of the simulated hydrometeor, but the current must in some way scale down with decreasing specimen size, and realistic graupel particles have length scales two orders of magnitude smaller than STS. Thus, we are skeptical about the applicability of the laboratory observed ice crystal ejection phenomena to the atmosphere.

However, the observations which originally motivated this study were done at $T_c \approx -10°C$ (Cheng, personal communication) with 2 mm diameter ice spheres. Though not quantitative, Cheng's results demonstrated that the phenomena is clearly evident in growth environments more representative of the atmosphere. The applicability of the underlying charge separation phenomenon at the molecular scale is unknown and deserves further study.

In a similar vein, it would be instructive to be able to compare these results directly to those of Jayaratne, et al.(1983). There are, however, great differences in the experiments and run conditions. The simulated hydrometeor in their experiments with ice crystal/rimer collisions has considerably less surface area (.0047 m^2) than our specimens (.07m^2 and .04m^2). Also, the riming rod achieves speeds of 10 m/sec with respect to the cloud chamber environment, whereas our buoyancy induced flow is of the order of .8 m/sec. And, of course, the importance of the large temperature and vapor gradient in our results adds another uncertainty. Though we obviously cannot make any direct comparisons, we can look at estimates of maximum current per unit area in the respective experiments. As presented in Jayaratne, et al (1983), the maximum current observed was about 10 pA. The unrimed surface area of the rod in that study was 47 cm^2, yielding a maximum current density of .21 pA/cm^2. On the other hand, in our experiment, we measured 12 pA current in one T_c=52°C run using STS. With a rough estimate of 50 cm^2 for the active ejection area on the sphere, we obtain a maximum current per unit area of .24 pA/cm^2. Interestingly, the values are comparable. Again, we cannot really conclude anything from this, as the experiments are so different.

Perhaps more interesting in a comparison with the work of Jayaratne, et al (1983), is a look at the polarity of the charge separation in the two experiments. In our study, the stainless steel simulated hydrometeor, which grows by vapor deposition and probably by riming as well, always charges positively at all T_S values and can temperatures. There is no regime in which the net charge transfer from the object is positive. This result is consistent with the observations of Caranti, et al. (1985), in which it was reported that frost growth estimated to be I micron thick was sufficient to charge a rimer-target positively.

In the work of Jayaratne, et al (1983), it appears that all runs begin with an initial 'pulse' of positive current to the rimed stainless steel rod, lasting from .5 to 1 minute. Contrary to our results, there are time periods during runs at temperatures below $\approx$ -15°C when the charge transfer to the rod is negative. As is evidenced in Baker, et al. (1987), though, an analysis of the processes operating in a chamber with a whirling rod growing by deposition and/or riming and impacting ice crystals also growing at the expense of supercooled water is complex, and it is difficult to confidently separate causes and effects. Therefore, again, we will not attempt to draw conclusions between the two experiments.

Without being quantitative, we can, however, speculate under what conditions electrically active ejection associated with frost growth might play a role in atmospheric charge separation. For a graupel particle in a dry growth regime in an updraft, it would seem that only a minimum layer of frost at most could be supported on the hydrometeor surface due to flow stresses on the delicate crystal structures. In such a situation, the surface

of the particle might be maintained in a state of continuous electrically active dry growth and ejection. Also, the transition from a dry to a wet growth regime could result in charge transfer similar to that seen in the ubiquitous melting signature.

The recommendations for future work are clear. It is necessary to definitively enunciate the relationship between the ejection of crystals and the separation of charge from the frost. For example, is the ice fragment ejection a process independent of and merely reflecting a separation of charge that already exists across the frost as a result of the surface dependent microphysics of deposition, or is ejection in itself the cause of current flow? (by virtue of ice fracture, for example.) To answer this, attention must be focused on methods of measuring the concentration of crystals emanating from a growing frosty specimen over time so that some quantitative estimates of the charge per crystal can be made. It is conceivable that the large increases of I_{max} with T_c (and ρ_c) are the result of increases in the numbers of ejected fragments alone. The charge per fragment may retain a substantial value even for $\nabla\rho$ & ∇T conditions appropriate for the atmosphere.

In solving the above, the problem of understanding the role of supercooled water and the riming process must also be addressed. In this work we have observed that charge separation is negligible in an environment in which a condensation sheath is not present. Similarly, In Jayaratne, et al (1983), significant currents were not measured when supercooled water was absent from the cloud chamber, and in the subsequent work of Baker, et al (1987), it was suggested that significant charging requires water saturation, but not

necessarily riming. Thus, it must be determined conclusively whether supercooled water is actively important in moderating the charge separation phenomena or if it is just maintaining the vapor gradient for ice growth by deposition.

And further, experiments must be done in which the temperature gradients and growth environment are realistic for hydrometeors growing in a thundercloud, and should be extended to a wind tunnel to examine the effects of realistic updraft velocities. Perhaps then firm conclusions about the importance of this phenomena to atmospheric charge separation can be made, and a better understanding of the electrical properties of the ice phase can be achieved.

Appendix A - Thermistor amplifier circuit

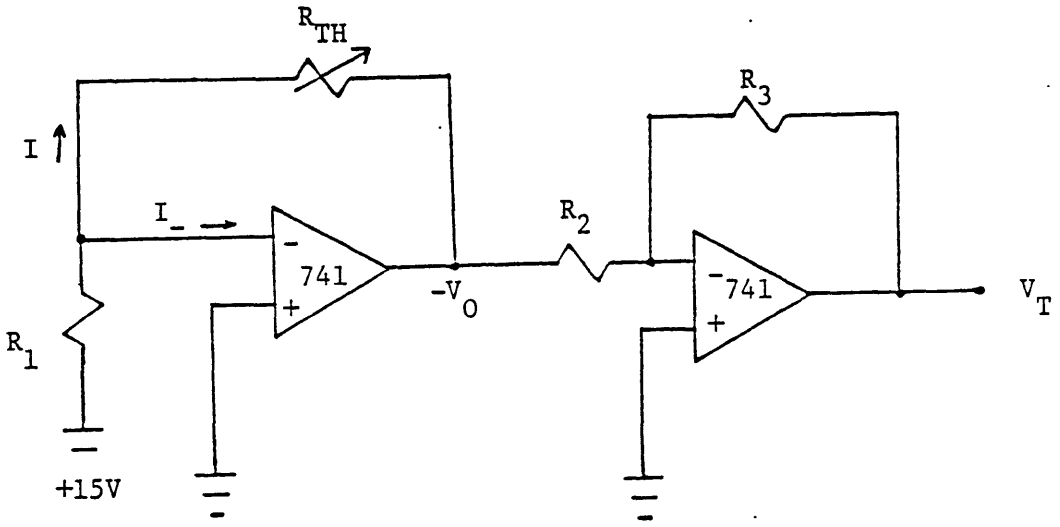

R_1 = .994 MΩ

R_2 = 12.1 KΩ

R_3 = 96.6 KΩ

$V_- \sim V_+ = GND$ and $I_- \sim 0$

$-V_O = I * R_{TH}$ and $I = \frac{15V}{.994M\Omega} \sim 15\,\mu A$

$$V_T = -\frac{R_3}{R_2} * V_O = -8 * V_O$$

So, $R_{TH} = 8333 * V_T$

Appendix B - Selected T_S runs with STS, T_C= 41°C, RH_S= 88%

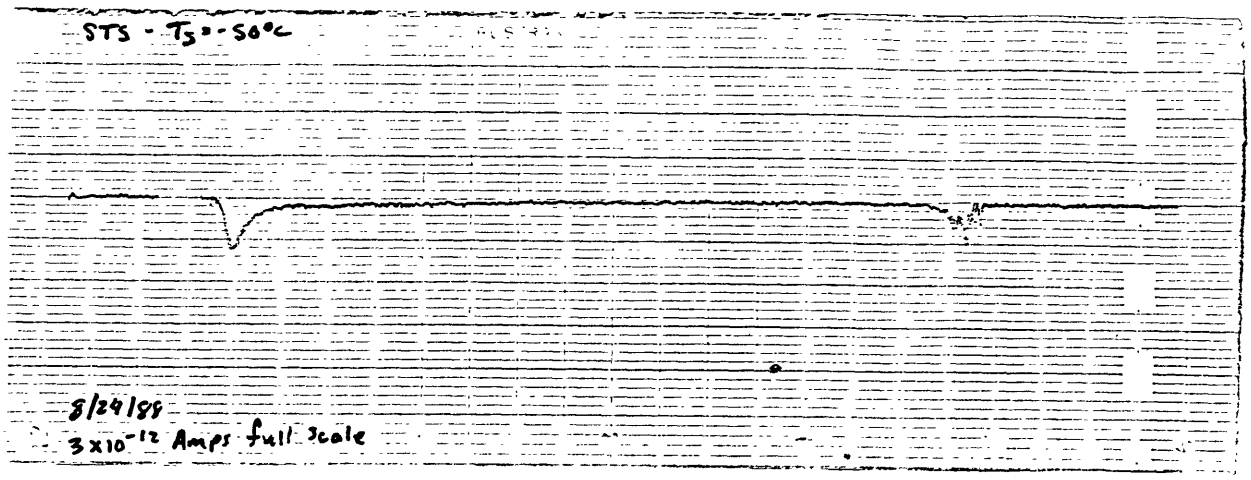

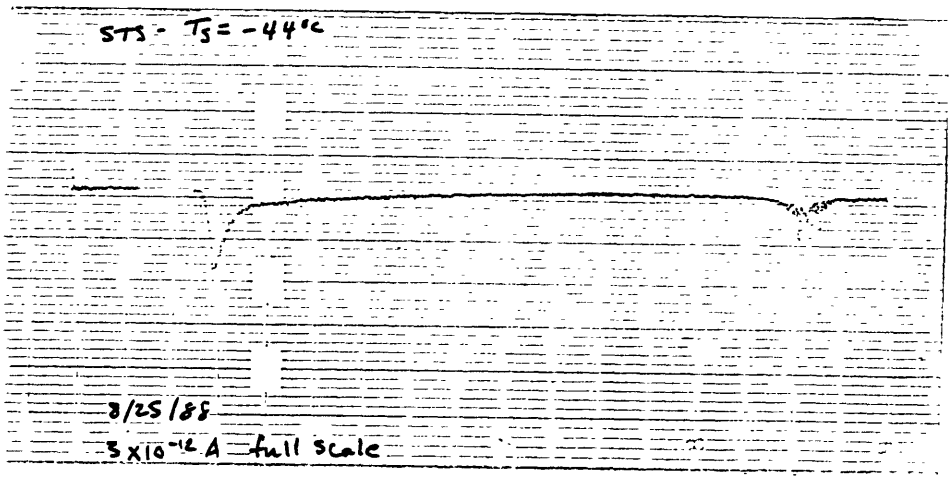

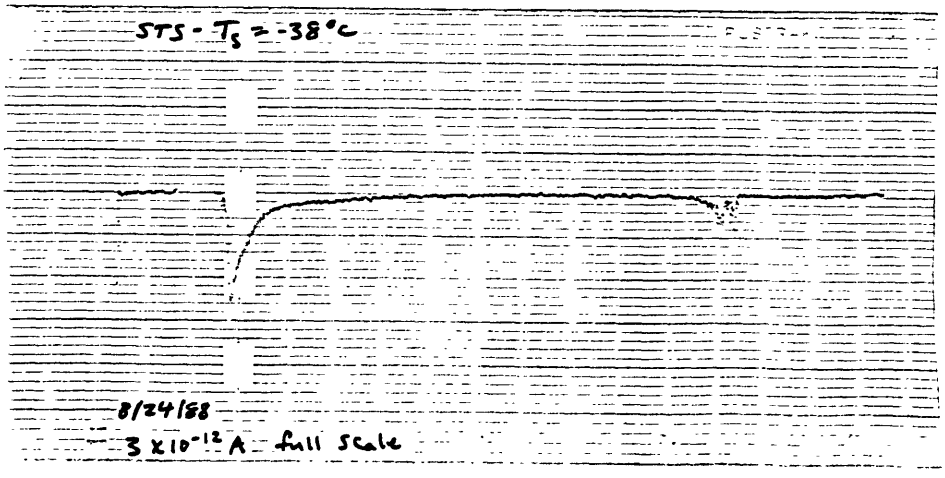

Appendix B (cont.) - Selected T_S runs with STS, T_C=41°C, RH_S= 88%

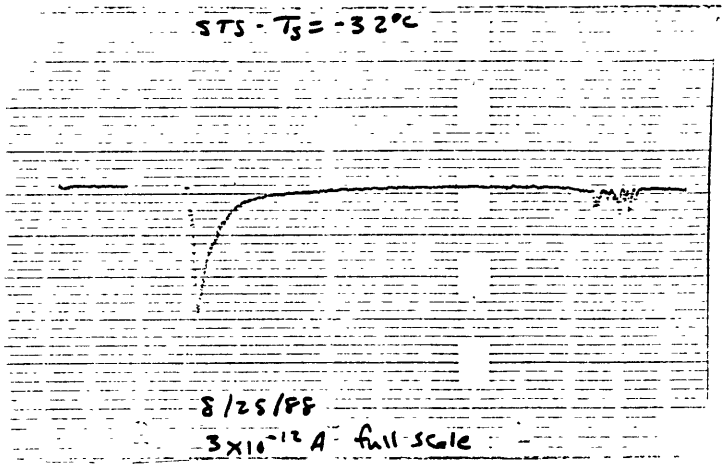

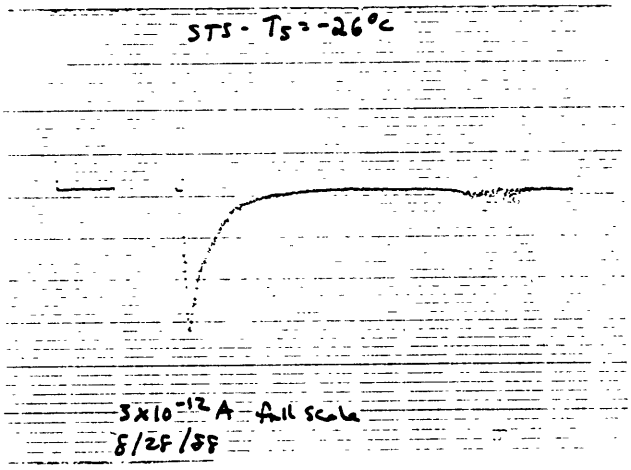

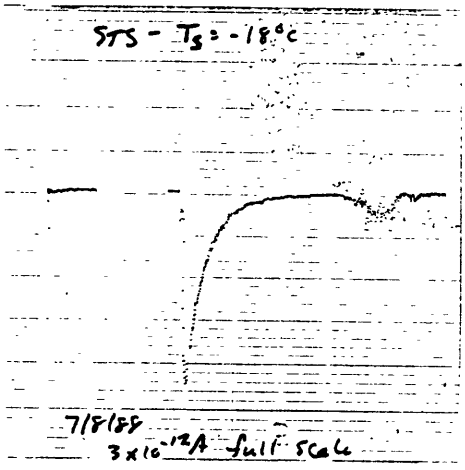

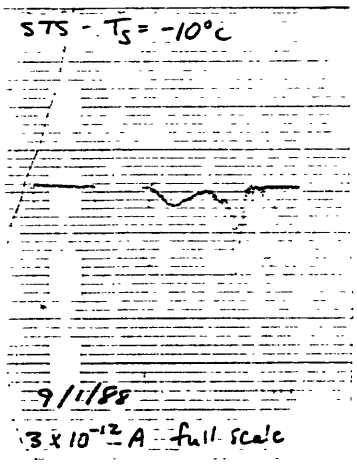

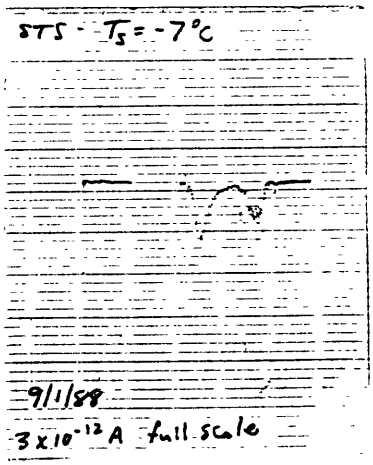

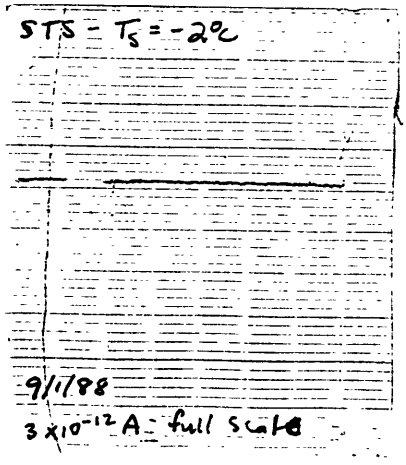

Appendix C - Selected T_S runs with STS, T_C= 52°C, RH_S = 84%

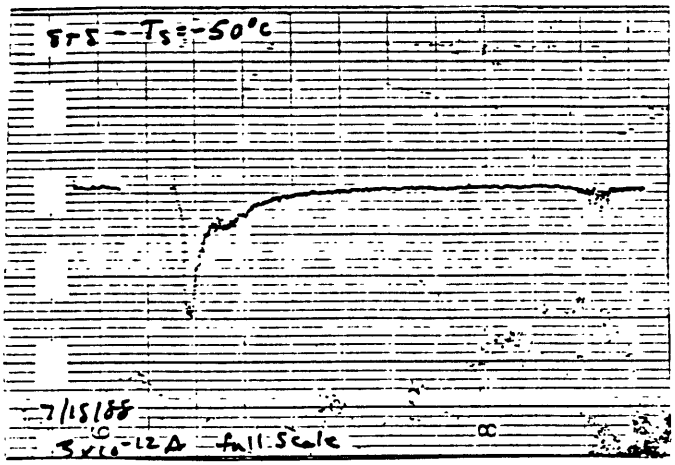

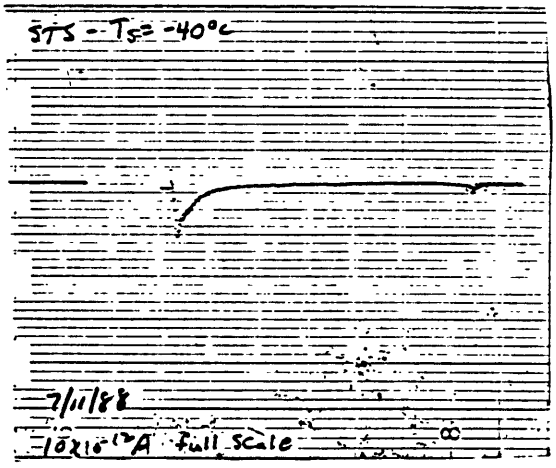

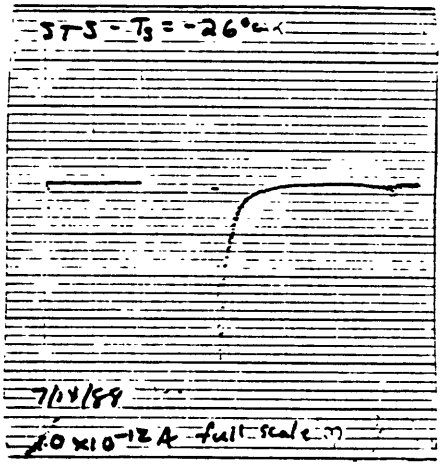

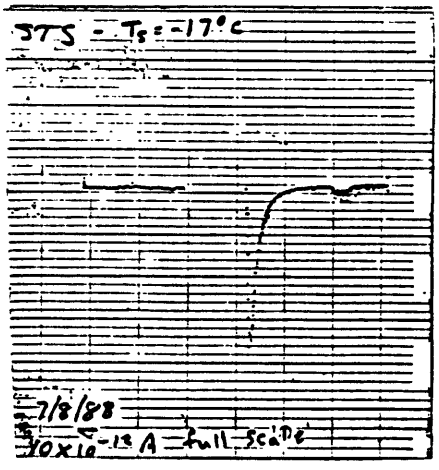

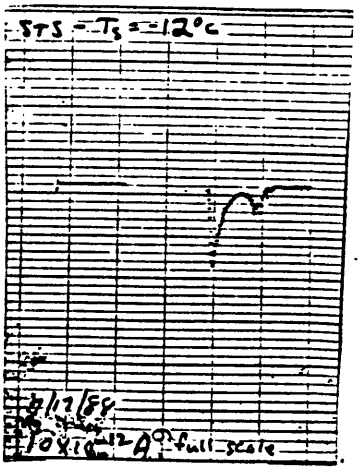

Appendix D - Boundary layer analysis

Mason's (1953) treatment involved solving the equation:

$$\partial\rho/\partial t = D\,[(\partial^2\rho/\partial r^2) + (2/r)(\partial\rho/\partial r)] \qquad (1D)$$

which has solution for $\rho(r)$ given by:

$$\rho_c - \rho(r) = [\rho_c - \rho(R)](R/r)[\,1 - \mathrm{erf}\{(r-R)/(2(Dt)^{1/2})\}] \qquad (2D)$$

with $R=.076$ m
$D= 2.1 \times 10^{-5}$ m^2/sec
$R/r \cong 1$

And, for T_c=41°C: $t = 2R/U \cong .2$ sec

For T_s=-17°C, $\rho(R) = \rho_{si}(-17°C) \cong 1$ g/m^3

So, for RH_{imax}=80%, $\rho_c \cong 45$ g/m^3 and (2D) reduces to:

$$\rho(r) = 45 - 44[\,1 - \mathrm{erf}\,(x)]$$

And for RH_{imax}=20%, $\rho_c \cong 11$ g/m^3 and (2D) becomes:

$$\rho(r) = 11 - 10[\,1 - \mathrm{erf}\,(x)]$$

where $x = (r - .076)/.0041$

Appendix D (cont.)

We can use the same equation, (1D), for the diffusion of heat in the boundary layer by substituting K for D. With $K \cong 2.1 \times 10^{-5}$ (from Gebhart, 1987), and the above environmental conditions, we get:

$$T(r) = 41 - 58[\ 1 - \text{erf}\ \{(r-.076)/(2(Kt)^{1/2})\}$$

The results are summarized in the Table below:

Table 1D - Boundary layer temperature and vapor profiles for two different RH runs at Tc=41°C, Ts=-17°C.

			RH_{Imax}=80%		RH_{Imax}=20%	
r (m)	T(r) °C	Psat(T) (mb)	$\rho(r)$ g/m^3	P(r) mb	$\rho(r)$ g/m^3	P(r) mb
.076	-17	1.4	1	1.4	1	1.4
.077	-1	5	13	16	4	5
.078	13	15	23	30	6	8
.079	24	30	32	44	8	11
.080	31	46	38	53	9	13
.081	36	62	41	58	10	14
.082	39	73	44	63	11	15
infinity	41	82	45	65	11	16

r = distance from center of sphere
T(r) = temperature in boundary layer
ρsat(T) = saturation vapor pressure at T
$\rho(r)$ = vapor density at r in boundary layer
P(r) = vapor pressure at r in boundary layer

Appendix E - Estimate of ΔT for graupel particle in atmosphere

For a simple estimate of ΔT for a graupel particle falling in a thunderstorm in a dry growth regime, neglecting the latent heat of deposition, we can approximate the heat balance by:

$$(\rho_S V C_S)d\ (\Delta T)/dt = -4\pi KRb(\Delta T) \quad (1E)$$

where $\Delta T = T_\infty - T_a$, T_∞ = ambient temperature

T_a = graupel temperature

R = graupel radius $\cong$ .25 cm

ρ_S = density of ice $\cong$ .8 g/cm^3

C_S = specific heat of ice $\cong$ .5 cal/g°C

K = thermal conductivity of air $\cong$ 6.0 X 10^{-5} cal/cmsec°C

b = ventilation coefficient $\cong$ 10

V = volume of graupel = $(4/3)\pi R^3$

All values are taken from Pruppacher & Klett (1980) for a large graupel particle. Solving (1E) yields:

$$\Delta T = (\text{const.})e^{-t/\alpha}$$

$$\text{where } \alpha = (R^2\rho_S C_S)/(3Kb)$$

Putting in the above numbers for α, the relaxation time, yields:

$$\alpha \cong 14 \text{ sec}$$

If we assume a moist lapse rate of 6°C/km and a fall speed of 5 m/sec for the graupel particle, then in 14 seconds, it will have traveled 70 meters. As an estimation of ΔT then, at some time=t, the graupel particle will have a temperature roughly corresponding to that of the atmosphere 14 seconds earlier, or 70 meters higher. Thus, an approximation for the temperature difference between the particle and its environment is just ΔT =(.07 km) * (6°C/km) = 0.4 °C. Thus:

$$\Delta T \cong 0.4\ ^{\circ}C$$

References

Baker, B., M.B. Baker, E.R. Jayaratne, J. Latham, and C.P.R. Saunders, 1987: The influence of diffusional growth rates on the charge transfer accompanying rebounding collisions between ice crystals and hailstones. *Quart. J. R. Met. Soc.*, **109**, 609-630.

Caranti, J.M., A.J. Illingworth, and S.J. Marsh, 1985: The charging of ice by differences in contact potential. *J. Geophys. Res.*, **90**, 6041-6046.

Cheng, R.J., 1973: The mechanism of multiplication process of glaciation in the atmosphere. Presented at the 8th International Conference on Nucleation, Leningrad, U.S.S.R.

Gebhart, B., 1988: *Buoyancy induced flows and transport.* Hemisphere Publishing Corporation, Washington, D.C.

Hallett, J., 1965: Field and Laboratory observations of ice crystal growth from the vapor. *J. Atmos. Sci.*, **22**, 64-69.

Jayaratne, E.R., C.P.R. Saunders, and J. Hallett, 1983: Laboratory studies of the charging of soft-hail during ice crystal interactions. *Quart. J. R. Met. Soc.*, **109**, 609-630.

Keller, V.W., 1980: Ice crystal growth in a dynamic thermal diffusion chamber. NASA Technical Paper 1651, 215 pp.

Latham, J., and B.J. Mason, 1961: Electric charge transfer associated with temperature gradients in ice. *Proc. Roy. Soc., A*, **260**, 523-536.

Latham, J., 1963: The electrification of frost deposits. *Quart. J. R. Met. Soc.*, **89**, 265-270.

Latham, J., and C.P. Stow, 1965: Electrification associated with the with the evaporation of ice. *J. Atmos. Sci.*, **22**, 320-324.

Latham, J., and C.P. Stow, 1966: The mechanism of charge transfer associated with the evaporation of ice. *J. Atmos. Sci.*, **23**, 245-247.

Mason, B.J., 1953: The growth of ice crystals in a supercooled water cloud. *Quart. J. R. Met. Soc.*, **79**, 104-111.

Pruppacher, H.R., & Klett, J.D., 1980: *Microphysics of clouds and Precipitation*, D. Reidel Publishing Co., Dordrecht, Holland.

Rogers, R.R., 1979: *A short course in cloud physics.* Pergamon Press, New York, NY.

Schaefer, V.J., and R.J. Cheng, 1971: The production of ice crystal fragments by sublimation and electrification. *J. de Rech. Atm.*, **5**, 5-10.

Sill, W.R., 1963: Noise in electrode systems. Master's Thesis, Massachusetts Institute of Technology, Cambridge, MA.